UNCLASSIFIED

SECURITY CLASSIFICATION OF THIS PAGE *(When Data Entered)*

REPORT DOCUMENTATION PAGE		READ INSTRUCTIONS BEFORE COMPLETING FORM
1. REPORT NUMBER U. of Iowa 84-20	2. GOVT ACCESSION NO.	3. RECIPIENT'S CATALOG NUMBER
4. TITLE *(and Subtitle)* WAVES AND INSTABILITIES IN COLLISIONLESS SHOCKS		5. TYPE OF REPORT & PERIOD COVERED Progress April 1984
		6. PERFORMING ORG. REPORT NUMBER
7. AUTHOR*(s)* DONALD A. GURNETT		8. CONTRACT OR GRANT NUMBER*(s)* N00014-76-C-0016
9. PERFORMING ORGANIZATION NAME AND ADDRESS Department of Physics and Astronomy The University of Iowa Iowa City, IA 52242		10. PROGRAM ELEMENT, PROJECT, TASK AREA & WORK UNIT NUMBERS
11. CONTROLLING OFFICE NAME AND ADDRESS Electronics Program Office Office of Naval Research Arlington, VA 22217		12. REPORT DATE April 1984 13. NUMBER OF PAGES 62
14. MONITORING AGENCY NAME & ADDRESS*(if different from Controlling Office)*		15. SECURITY CLASS. *(of this report)* UNCLASSIFIED 15a. DECLASSIFICATION/DOWNGRADING SCHEDULE

16. DISTRIBUTION STATEMENT *(of this Report)*

Approved for public release; distribution is unlimited.

17. DISTRIBUTION STATEMENT *(of the abstract entered in Block 20, if different from Report)*

18. SUPPLEMENTARY NOTES

To be published in Collisionless Shock Waves in the Heliosphere, ed. by B. Tsurutani and R. Stone, AGU, Washington, DC, 1984.

19. KEY WORDS *(Continue on reverse side if necessary and identify by block number)*

Collisionless shocks
Waves
Instabilities

20. ABSTRACT *(Continue on reverse side if necessary and identify by block number)*

(see following page)

DD FORM 1 JAN 73 1473 EDITION OF 1 NOV 65 IS OBSOLETE
S/N 0102-LF-014-6601

UNCLASSIFIED

SECURITY CLASSIFICATION OF THIS PAGE *(When Data Entered)*

Department of Physics and Astronomy

THE UNIVERSITY OF IOWA

Iowa City, Iowa 52242

U. of Iowa 84-20

WAVES AND INSTABILITIES IN COLLISIONLESS SHOCKS

by

Donald A. Gurnett

Department of Physics and Astronomy
The University of Iowa
Iowa City, IA 52242

Invited paper presented at the Chapman Conference on Collisionless Shocks, Napa, California, February 20-24, 1984.

To be published in Collisionless Shock Waves in the Heliosphere, ed. by B. Tsurutani and R. Stone, AGU, Washington, DC, 1984.

ABSTRACT

By scattering particles and causing dissipation, waves in a collisionless shock play a role similar to collisions in an ordinary gas. In describing the waves and instability that occur near a shock three regions must be considered: (1) the transition region, (2) the upstream region, and (3) the downstream region. The transition region is usually characterized by an abrupt broadband burst of electrostatic noise extending to frequencies well above the ion plasma frequency, and by a broadband burst of whistler-mode electromagnetic noise at frequencies below the electron cyclotron frequency. The burst of electrostatic noise is believed to be the primary mechanism by which heating and dissipation takes place at the shock. This noise is believed to be ion-acoustic noise driven either by a current or an electron beam in the shock. Electrostatic lower-hybrid waves are also sometimes observed in the transition region. These waves are excited by ions reflected by the shock, and can be very effective at heating both ion and electrons.

Upstream of the shock electron plasma oscillations, ion-acoustic waves, and intense ULF (ultra-low-frequency) magnetohydrodynamic waves are frequently observed. The electron plasma oscillations occur in the electron foreshock and are driven by suprathermal electrons escaping into the region upstream of the shock. Both the ion-acoustic and ULF waves occur in the ion foreshock and are associated with ions streaming into the region upstream of

the shock. The region downstream of the shock is usually very chaotic. Electrostatic waves, similar to the broadband noise in the transition region but less intense, often extends long distances into the downstream region. Whistler-mode emissions also frequently are observed in the downstream region. Some of these waves may be locally generated, and others may be convected downstream from the shock.

This paper reviews all of the above waves and comments on the similarities between waves observed near the bow shocks of earth, Venus, Jupiter and Saturn, and interplanetary shocks. Possible mechanisms for generating each type of wave are also considered.

I. INTRODUCTION

Shock waves are characterized by an abrupt density change in a thin dissipative layer that propagates through the fluid. In the dissipation layer energy associated with the ordered flow is irreversibly converted into disordered thermal energy. In an ordinary gas this energy transfer is caused by collisions between molecules in the gas. In a tenuous plasma, where collisionless are essentially negligible, the energy transfer is caused by wave-particle interactions. The first evidence of collisionless shocks was obtained from spacecraft observations in the solar wind upstream of the earth's magnetosphere [Ness et al., 1964]. Collisionless shock waves have also been produced in laboratory plasmas [Paul et al., 1965]. Since the discovery of collisionless shocks, the central question has been to explain how the dissipation can occur in an essentially collisionless gas. It is now widely recognized that waves generated by instabilities in the shock transition region act to heat the plasma via wave-particle interactions, thereby producing dissipation. Wave-particle interactions therefore play a role similar to collisions in an ordinary gas. The purpose of this chapter is to review spacecraft observations of waves associated with collisionless shocks and discuss the origin of these waves. This review only considers the waves responsible for the dissipation, and does not attempt to describe the quasi-stationary waves that make up the shock transition itself.

Although the importance of waves and instabilities in collisionless shocks was recognized in many early theoretical analyses, it was not until the launch of the OGO series of satellites that suitable measurements were available to confirm the existence of these waves. The first observations of magnetic field turbulence associated with the earth's bow shock were obtained by Holzer et al. [1966], and the first electric field observations were obtained by Fredricks et al. [1968; 1970]. Of these the electric field measurements of Fredricks et al. are particularly important because they demonstrated that electrostatic turbulence was responsible for the plasma heating and dissipation in the shock.

Since the early OGO observations many measurements have been made of plasma wave turbulence in collisionless shocks. These include measurements at the bow shocks of four planets, Venus, Earth, Jupiter and Saturn, and the detection of shock waves in the interplanetary medium. It is not possible, or even desirable, to give a full chronological account of all of the individual contributions to this area of research. Instead, what we will attempt to do is present the main features of the observations in as systematic a manner as possible. The discussion will be organized into three distinct topics: (1) the transition region, (2) the upstream region, and (3) the downstream region. In each region we will attempt to characterize the electric and magnetic field spectrums, comment on the factors that control the variability of the noise, and discuss the various interpretations of the instabilities involved.

II. THE SHOCK TRANSITION REGION

Because the transition region is where the main heating takes place, we first concentrate our attention on this region. Figure 1 shows the electric and magnetic fields detected by ISEE-1 during a typical crossing of the earth's bow shock. This crossing occurred on December 13, 1977, at a magnetic local time of 8.2 hr. and a geocentric radial distance of 16.7 R_E. The shock in this case was a quasi-perpendicular, super-critical, turbulent shock. For a further discussion of this particular shock, see Feldman et al. [1982].

As can be seen from Figure 1, an abrupt burst of electric and magnetic field noise occurs as the magnetic field changes from the upstream value of about 6 nT to the downstream value of about 15 nT. This region is called the transition region. Both the electric and magnetic field noise extend over a broad frequency range, from below 5 Hz to about 10 kHz for the electric field, and from below 5 Hz to about 300 Hz for the magnetic field. The electric field spectrum remains relatively flat over a large frequency range, whereas the magnetic field spectrum drops rapidly with increasing frequency. The upper frequency limit of the magnetic field noise is near the electron cyclotron frequency, f_{ce}, which varies from about 170 Hz in the upstream region to about 420 Hz in the downstream region. The upper frequency limit of the electric field noise is near the electron plasma frequency, f_{pe}, which varies from about 15 kHz in the upstream region to

about 28 kHz in the downstream region. For both the electric and magnetic field noise the region of highest intensity lasts about 30 seconds, with the peak intensities roughly centered on the ramp in the magnetic field. The magnetic noise is almost entirely confined to within one minute of the shock. The electric field noise on the other hand extends far into the downstream region.

The electric and magnetic field intensities shown in Figure 1 are typical of quasi-perpendicular shocks. Quasi-perpendicular shocks are shocks for which the angle between the upstream magnetic field and the shock normal, θ_{Bn}, is greater than 45° [Greenstadt and Fredricks, 1979]. For θ_{Bn} less than about 45° the shock structure is dominated by nonlocal effects arising from particles and waves propagating into the upstream region. Shocks with θ_{Bn} less than 45° are called quasi-parallel shocks [Greenstadt and Fredricks, 1979]. For quasi-parallel shocks it is sometimes not possible to clearly identify a shock transition. An example of a quasi-parallel shock is discussed later.

The plasma wave intensities observed in the earth's bow shock vary considerably from event to event. Some typical shock spectrums are illustrated in Figure 2, which is taken from Rodriguez and Gurnett [1975]. This illustration shows the electric and magnetic field spectrums from 36 shock crossing selected at random from the IMP-6 spacecraft data. Most of these spectrums are for quasi-perpendicular shocks, although a few (~ 15%) are for quasi-parallel shocks. Each spectrum gives the spectral density averaged over an interval of 5.12 sec at the time of maximum intensity. As can be seen, the intensities vary over a large range, up to 4 orders of magnitude

for the electric field and 2 orders of magnitude for the magnetic field. The r.m.s. field strength, integrated over the frequency range shown, varies from about 0.19 to 4.0 $mV \cdot m^{-1}$ for the electric field and from about 4.6 to 84 pT for the magnetic field. The field intensities fluctuate considerably on short time scales. When averaged over intervals of 0.1 sec, the peak field strengths are typically 3 to 10 times larger than those shown in Figure 2.

Usually the magnetic field spectrum decreases monotonically with increasing frequency, varying approximately as $f^{-4.0\pm0.5}$ [Rodriguez and Gurnett, 1975]. The spectrum tends to steepen somewhat above about 100 Hz, and drops below the instrument noise level at frequencies about a few hundred Hz. This trend can be seen in several of the magnetic spectrums shown in Figure 2. Careful inspection of the electric field spectrums shows that the electric field spectrum consists of two components: a low frequency component below a few hundred Hz, varying approximately as $f^{-2.0\pm1.0}$, and a high frequency component with a broad peak at about one kHz. The general form of these various components is summarized in Figure 3. The low frequency magnetic noise and the low frequency component of the electric field noise are believed to be due to electromagnetic whistler mode waves [Rodriguez and Gurnett, 1975]. The high frequency electric field noise consists of electrostatic waves since no magnetic component can be detected.

In addition to the spectrums from the earth's bow shock, electric field spectrums have also been obtained from the bow shocks of three other planets: Venus, Jupiter and Saturn. The electric field spectrums from all four planets have been compared by Scarf et al. [1981], and are summarized

in Figure 4. The measurements at Jupiter and Saturn are from Voyagers 1 and 2, and the measurements at Venus are from the Pioneer Venus Orbiter. Although the measurements are not identical in all cases, the electric field spectrums show a remarkably close similarity, particularly for Earth, Jupiter and Saturn. The spectrums at these three planets show evidence of both low frequency and high frequency components, and have rather similar intensities. The upper frequency cutoff of the high frequency component varies in direct proportion to the electron plasma frequency, which varies inversely with the radial distance from the sun. The main difference in the spectrums is that the high frequency component at Jupiter and Saturn appears to be more sharply peaked and more clearly separated from the low frequency component than at the earth.

The Pioneer Venus spectrums differ somewhat from the spectrums at Earth, Jupiter and Saturn. Usually the spectrums at Venus are more intense and decrease monotonically with increasing frequency, with no evidence of high and low frequency components. Some of these differences may be due to instrumental effects. The Pioneer Venus instrument [Scarf et al., 1980] has poorer frequency resolution (only four frequencies) and lower sensitivity than either the IMP-6 or Voyager instruments. With only four frequency channels it would be difficult to distinguish the high and low frequency components evident in the IMP-6 and Voyager data.

Plasma wave turbulence similar to that observed at planetary bow shocks has been reported in association with interplanetary shocks by a number of investigators, including Scarf et al. [1974], Neubauer et al. [1977], Scarf [1978], Gurnett et al. [1979], and Kennel et al. [1982]. Interplanetary

shocks can be produced either by flares at the sun, or by co-rotating high speed streams [Hundhausen, 1972]. Since co-rotating shocks are relatively rare at 1 AU, almost all of the plasma wave observations are for shocks produced by solar flares. The plasma wave turbulence associated with interplanetary shocks is very similar to the turbulence observed at planetary bow shocks. Usually the turbulence consists of a low frequency electromagnetic component, believed to be whistler mode waves, and a high frequency electrostatic component extending up to near the electron plasma frequency. Although the types of waves observed at interplanetary shocks are very similar to those observed at planetary shocks, the intensities are usually lower, particularly for the high frequency electrostatic component. This difference is illustrated in Figure 5 which shows the electric and magnetic field spectrums for a series of interplanetary shocks detected by the ISEE-3 spacecraft at 1 AU. The electric and magnetic field turbulence of these shocks has been previously discussed by Kennel et al. [1982]. By comparing these spectrums with the IMP-6 spectrums in Figure 2, it can be seen that the electric field intensities of the interplanetary shocks are about two to three orders of magnitude lower than for the earth's bow shock. The magnetic field intensities, on the other hand, are rather similar. The reason for the lower electric field intensities is probably related to the shock strength. Usually interplanetary shocks have much lower Mach numbers than planetary bow shocks. For example, the average Mach number of the interplanetary shocks in Figure 5 is only 2.6, whereas for the bow shocks in Figure 2 the average Mach number is 7.8.

It is evident from the above examples that the intensity of the plasma wave turbulence associated with collisionless shocks varies considerably from event to event. Even after nearly twenty years of study the factors that control the intensities are only partially understood. The only systematic investigation of the relation between the upstream parameters and the wave intensities is the study carried out by Rodriguez and Gurnett [1976]. In their study, a total of 96 shocks detected by IMP-6 were used to determine the correlation between three plasma wave intensities and twelve upstream plasma parameters. The plasma wave intensities used were (1) the r.m.s. field strength, E_L, of the low frequency electric field noise, (2) the r.m.s. field strength, E_H, of the high frequency electrostatic noise, and (3) the r.m.s. field strength, B_L, of the low frequency magnetic noise. The field strengths E_L and E_H were computed by integrating the electric field spectrums from 20 Hz to 200 Hz and 200 Hz to 4 kHz, and B_L was computed by integrating the magnetic field spectrum from 20 Hz to 4 kHz. The upstream plasma parameters used were the Alfven Mach numbers, M_A; the sonic Mach number, M_S; the solar wind velocity, V_{sw}; the plasma number density, N; the electron and ion temperatures, T_e and T_i; the electron to ion temperature ratio, T_e/T_i; the plasma energy density to magnetic energy density ratio, β; the magnetic field strength, $|\vec{B}|$; and the angle between the magnetic field and the shock normal, θ_{Bn}. For each combination of plasma wave intensity and upstream plasma parameter, the linear correlation coefficient was computed between the logarithm of the plasma wave intensity and the upstream parameter. The logarithm of the plasma wave intensity was used because the dynamic range is usually so large that the intensities

cannot reasonably be represented by a linear parameter. The resulting correlation coefficients are summarized in Table 1.

As can be seen from Table 1, the highest correlation coefficient listed, 0.60, is between the high frequency component of electric field, E_H, and the electron to ion temperature ratio, T_e/T_i. A scatter plot of these two parameters is shown in Figure 6. This plot clearly shows that the electric field intensity of the high frequency electrostatic noise increases as T_e/T_i increases. Another parameter that appears to have an important influence is the shock normal angle, θ_{Bn}, which is correlated with both the electric and magnetic field amplitude of the low frequency electromagnetic noise.

A. Interpretation of the High Frequency Electrostatic Noise

We now consider the various instability mechanisms that have been proposed to explain the high frequency electrostatic noise. The instability responsible for this noise has been controversial ever since its discovery by Fredricks et al. [1968]. The instabilities that could possibly be responsible for this noise are (1) a Buneman mode instability, (2) a current-driven ion-acoustic instability, (3) an ion-beam instability, and (4) an electron-beam instability. The main interpretational difficulty has to do with the rest frame frequency of the waves. Because the wavelength of the electrostatic waves can be very short, the Doppler shift due to the motion of the solar wind can be very large, in some cases much larger than the rest frame frequency. Since the wavelength cannot be directly measured, the rest frame frequency is unknown. This makes it impossible to uniquely identify the plasma wave mode on the basis of the frequency spectrum alone.

First, we consider the Buneman instability. This instability is an electrostatic instability caused by a relative drift between the electrons and ions, as would be expected in the current layer associated with the magnetic ramp. The Buneman instability occurs over a broad range of frequencies centered on the Buneman frequency, $f_B = (1/2)(m_e/2\ m_i)^{1/3} f_{pe}$. This frequency is indicated at the bottom of Figure 3. Because the Buneman mode has relatively long wavelengths, the Doppler shift is small. The observed frequency is then essentially the same as the rest frame frequency. As can be seen in Figure 3 the Buneman frequency is in good agreement with the peak in the spectrum of the high frequency electrostatic noise. The broad bandwidth of the high frequency electrostatic noise is also in agreement with the broad bandwidth expected for the Buneman mode. Thus, on the basis of the frequency spectrum alone the Buneman instability would appear to be a good candidate. The main difficulty with the Buneman instability is that a very large drift velocity, much greater than the electron thermal velocity, is required before the instability occurs. Both plasma and magnetic field measurements show that such large drift velocities do not occur in the transition region. Thus, although the frequency and bandwidth are in the proper range, the Buneman instability is not regarded as a viable mechanism for generating the high frequency electrostatic noise.

Next, we consider the current-driven ion-acoustic instability. This instability is also driven by a drift between the electrons and ions. The threshold drift velocity for this instability is strongly dependent on the electron to ion temperature ratio [Stix, 1962]. When T_e/T_i is near one the threshold is very high, comparable to the electron thermal velocity. As

T_e/T_i increases, the threshold drops very rapidly, approaching the ion thermal speed for $T_e/T_i \gg 1$. As discussed earlier, the intensity of the high frequency electrostatic noise is closely correlated with T_e/T_i, increasing rapidly for $T_e/T_i \gg 1$. This correlation provides a strong indication that the current-driven ion-acoustic instability may be responsible for the noise. However, we must also consider the frequency spectrum. It is well-known that the rest frame frequency of the ion-acoustic mode is always below the ion plasma frequency, f_{pi}. As can be seen from Figure 3, the frequency spectrum extends well above f_{pi}, apparently in disagreement with an ion-acoustic interpretation. However, when the drift velocity is well above threshold, the wavelengths excited by the ion-acoustic instability are very short, $\lambda \gtrsim 2\pi\lambda_D$, where λ_D is the Debye length. Wavelengths shorter than $\lambda \simeq 2\pi\lambda_D$ are strongly damped by ion Landau damping [Krall and Trivelpiece, 1973]. Because of the short wavelength, the Doppler shift for the ion-acoustic mode is very large, much larger than the rest frame frequency. The maximum Doppler shift is given by $V_{sw}/2\pi\lambda_D$, where V_{sw} is the solar wind velocity. For typical conditions in the solar wind at the earth (V_{sw} = 400 km s^{-1}, N = 5 cm^{-3}, and $T_e = 1.4 \times 10^5$°K), the maximum Doppler shift frequency is about 6 kHz. As can be seen in Figure 3, the maximum Doppler shift, $V_{sw}/2\pi\lambda_D$, is in good agreement with the upper cutoff of the high frequency electrostatic noise. Because the Debye length depends on the electron density, it can be shown that the maximum Doppler shift decreases inversely with increasing radial distance from the sun. As can be seen in Figure 4, the upper cutoff frequency of the electrostatic noise at Earth, Jupiter and Saturn follows this trend, decreasing inversely with increasing

radial distance from the sun. Note that the maximum Doppler shift and the electron plasma frequency vary in essentially the same way (for a constant solar wind velocity and temperature both vary as $\sqrt{n_e}$). In the ion-acoustic interpretation it is only coincidental that the upper cutoff is near the electron plasma frequency since the plasma frequency is not related to the upper cutoff frequency.

Although the above comparisons provide substantial evidence that the high frequency electrostatic noise is caused by ion-acoustic waves, there are nevertheless substantial difficulties. As can be seen in Figure 6, many cases exist for which $T_e/T_i \simeq 1$ to 2. Under these conditions strong ion Landau damping should stabilize the ion-acoustic mode. Several suggestions have been made for avoiding this difficulty. The T_e/T_i values in Figure 6 are for the undisturbed solar wind ahead of the shock. Usually the electron temperature starts to increase well before the main ramp in the shock is encountered. This increase in electron temperature lowers the instability threshold in the transition region compared to what would be predicted from the upstream T_e/T_i ratio. Also, Priest and Sanderson [1972] have shown that the growth rate of the ion-acoustic instability is enhanced by the electron temperature gradient that exists ahead of the shock.

The third basic mechanism for generating the high frequency electrostatic noise is an ion-beam instability. This mechanism is suggested by the fact that for quasi-perpendicular shocks the onset of the high frequency electrostatic noise is often correlated with the appearance of ions reflected by the shock. This effect is illustrated in Figure 7, which shows the reflected ion density, n_I, for a quasi-perpendicular shock analyzed by

Paschmann et al. [1982]. As can be seen, the onset of the high frequency electrostatic noise occurs well ahead of the main part of the magnetic ramp and coincides almost exactly with the onset of the reflected ions gyrating ahead of the shock. This relationship is typical of super-critical quasi-perpendicular shocks and strongly indicates that the reflected ions provide the free energy for the high frequency electrostatic noise, at least for this type of shock. It is well known that ion beams can excite both ion-acoustic waves [Tidman and Krall, 1971] and short wavelength ion beam modes [Lemons et al., 1979]. However, these ion-beam driven instabilities also have a threshold electron to ion temperature ratio, $T_e/T_i \gtrsim 5$, which is often difficult to satisfy. Thus, the ion-beam instability mechanism has the same difficulty that was encountered in the current-driven ion-acoustic instability.

Finally, we discuss an electron beam mechanism for generating the high frequency electrostatic noise. This mechanism, which was first proposed by Thomsen et al. [1983], is based on the recent discovery of an electron beam in the shock transition region [Feldman et al., 1982]. This electron beam is illustrated in Figure 8 which shows a series of parallel cuts of the electron distribution function upstream of the shock, in the transition region, and downstream of the shock. The beam, which can be seen in the transition region distribution, is directed toward the downstream region and is believed to be produced by an electrostatic potential difference across the shock. Typical beam energies range from about 50 to 150 eV. Because the beam produces a region with a large positive slope in the reduced distribution function, $\partial F/\partial v_{\parallel} > 0$, the plasma is unstable to electrostatic waves. Thomsen et al. [1983] have performed a detailed stability analysis

and have concluded that two unstable modes can occur: (1) an ion-acoustic mode with frequencies slightly below the ion plasma frequency, and (2) an electron-acoustic mode with frequencies several times the ion plasma frequency. The ion-acoustic waves have very short wavelengths, $k\lambda_D \lesssim 0.4$, which implies Doppler shifts sufficiently high to account for the frequency spectrum of the high frequency electrostatic noise. The electron-acoustic waves have longer wavelengths, $k\lambda_D \lesssim 0.14$, and smaller Doppler shifts. The rest frame frequencies of these waves extend up to approximately 10 f_{pi}, which is sufficiently high to account for most of the observed spectrum even without considering Doppler shifts. The ion-acoustic mode has a slightly higher growth rate than the electron-acoustic mode, but both instabilities grow sufficiently rapidly to generate large amplitude waves in the transition region. Therefore, these electron beam driven instabilities appear to be good candidates for explaining the high frequency electrostatic noise. Compared to the other instabilities discussed, they have the desirable feature of operating for low electron to proton temperature ratios, $T_e/T_p \gtrsim 1$.

B. Alternative Interpretations of the Low Frequency Electric and Magnetic Field Noise

The low frequency magnetic field noise was first interpreted as whistler mode turbulence by Olsen et al. [1969]. The presence of a magnetic field clearly indicates an electromagnetic wave, and in the frequency range, $f_{ci} < f < f_{ce}$, the only known electromagnetic mode is the whistler mode. The main interpretational question involves the low frequency component of the electric field. Rodriguez and Gurnett [1975] interpreted the electric

field as the electric component of whistler mode noise. This interpretation is consistent with most of the observed characteristics. First, simple inspection of the electric and magnetic field plots, such as in Figure 1, shows that at low frequencies, $f \leq 100$ Hz, the temporal variations of the electric and magnetic fields are very similar. Both have smooth temporal variations, occur on similar time scales, and have about the same dynamic range. Second, the spectral shapes are similar, with $E_L^2 \sim f^{-2.0\pm1.0}$ and $B_L^2 \sim f^{-4.0\pm0.5}$, and the magnetic to electric field ratio is reasonably consistent with the whistler mode, which predicts that $cB_L/E_L \sim f^{-1/2}$. The only serious difficulty is with the magnitude of the magnetic to electric field ratio. For propagation parallel to the magnetic field, the magnetic to electric field ratio is given by $cB_L/E_L = f_{pe}/(f_{ce}f)^{1/2}$. For typical conditions in the Earth's bow shock (f_{pe} = 20 kHz, and f_{ce} = 140 Hz) a representative value for cB_L/E_L is 320 at f = 31 Hz. At f = 31 Hz, Rodriguez and Gurnett [1975] give cB_L/E_L values ranging from about 10 to 30. The electric field is therefore stronger than would be expected for parallel propagation. A similar result has been reported for interplanetary shocks by Coroniti et al. [1982]. This disagreement could either indicate that an additional electrostatic component is present, or that the whistler mode waves are propagating at a large angle to the magnetic field. At large wave normal angles, near the resonance cone, the whistler mode becomes quasi-electrostatic, which would tend to reduce the cB_L/E_L ratio.

The possibility that the low frequency electric field noise could have a significant electrostatic component has been given added importance by a recent Prognoz-8 report of electrostatic lower-hybrid noise in the earth's bow shock [Vaisberg et al., 1983]. The Prognoz-8 spacecraft has the

capability of making electric field measurements down to 0.3 Hz, well below the frequency range of the IMP-6 and ISEE-1 instruments. A spectrum of the noise detected by Prognoz-8 is shown in Figure 9. This spectrum has the same general frequency dependence and intensity as the low frequency electric field component detected by IMP-6 and ISEE-1, but has the new feature of exhibiting a well-defined peak near the lower hybrid resonance frequency, $f_{LHR} = \sqrt{f_{ce} f_{ci}}$. In the transition region f_{LHR} is typically in the range from about 3 to 10 Hz.

A number of investigators have considered the possibility of electrostatic instabilities near the lower hybrid resonance frequency [McBride et al., 1972; Davidson and Gladd, 1975; Huba and Wu, 1976; Hsia et al., 1979; Wu et al., 1982]. The essential feature of this instability is that electrostatic oscillations can be excited near the lower-hybrid resonance frequency by a variety of unstable electron and ion distribution functions. Many variants of this instability have been proposed. For a review of these instabilities, see Winske [1984]. For the bow shock, Vaisberg et al. [1983] have suggested that reflected ions provide the free energy to drive the instability. The presence of lower hybrid waves in the transition region could be quite important because these waves are very effective for heating both electrons and ions. An important question that remains to be answered is the relationship of the lower hybrid waves to the whistler mode turbulence in the shock. It is well known [Stix, 1962] that the lower hybrid resonance is a limiting case of the whistler mode. Near the resonance cone, the whistler mode becomes quasi-electrostatic for frequencies extending from f_{LHR} to f_{ce}. This frequency range corresponds very well with the frequency

range of the low frequency electric field noise (see Figure 3). Once generated quasi-electrostatic lower-hybrid waves can be converted to electromagnetic whistler mode waves if the wave vector is refracted away from the resonance cone by suitable plasma density gradients. Thus, it is possible that a lower-hybrid instability could account for some or all of the low frequency electromagnetic noise.

Various mechanisms for generating whistler mode noise via resonant interactions have been considered by Tokar et al. [1984]. The most obvious free energy source is the electron beam shown in Figure 8. Three resonant interactions were considered: (1) a Landau resonance at $v_{\parallel} = \omega/k_{\parallel}$, (2) a cyclotron resonance at $v_{\parallel} = (\omega - \omega_{ce})/k_{\parallel}$, and (3) an anomalous cyclotron resonance at $v_{\parallel} = (\omega + \omega_{ce})/k_{\parallel}$. For the Landau resonance the free energy source is the region of positive slope, $\partial f/\partial v_{\parallel} > 0$, in the beam, whereas for the cyclotron and anomalous cyclotron resonances the free energy is the $T_{\perp} > T_{\parallel}$ anisotropy in the electron beam (see Figure 8). Of these, the Landau and anomalous cyclotron resonances do not give adequate wave growths. The reason for the small growth rates is mainly due to the fact that the waves are generated with wave vectors directed toward the downstream region. Since the waves propagate in the direction of plasma flow, they spend too little time in the transition region for large wave growth to occur. On the other hand, for the cyclotron resonance the waves are generated with wave vectors directed toward the upstream region, against the plasma flow. For certain combinations of frequencies and wave vector directions, these waves spend a long time in the transition region and can grow to very large amplitudes. Growth rate computations performed by Tokar et al. [1984] show that whistler mode waves generated by cyclotron resonance interactions with the electron

beam grow to large amplitudes (10 e-foldings) over a frequency range from about 5 to 85 Hz. These amplitudes and frequencies appear to be satisfactory to explain the main features of the whistler mode noise observed in the shock.

III. THE UPSTREAM REGION

Because both suprathermal electrons and ions stream into the solar wind ahead of the shock, it is not surprising that waves and instabilities are also observed upstream of the shock. To organize the discussion of these waves it is useful to distinguish two regions, called the electron foreshock and the ion foreshock. Because the particles ejected into the solar wind are moving relatively slowly, the motion of the solar wind has a significant effect on the trajectories of the particles. It is easy to show from time of flight considerations that a boundary exists ahead of which essentially no particles are observed. These boundaries are shown by the dashed lines in Figure 10. The region behind the electron boundary is called the electron foreshock, and the region behind the ion boundary is called the ion foreshock. Because the electrons are moving faster, the electron foreshock boundary is located upstream of the ion foreshock boundary. For a further discussion of the dynamical effects responsible for these boundaries see Greenstadt and Fredricks [1979].

The electron and ion foreshock boundaries are easily identified in the plasma wave data. A typical example in which both boundaries are clearly evident is shown in Figure 11. In this case the electron foreshock boundary is encountered at about 1908 UT and is characterized by an abrupt onset of electron plasma oscillations at the electron plasma frequency. Electron plasma oscillations and their association with nonthermal, few keV, electrons streaming into the solar wind from the bow shock were first reported

by Scarf et al. [1971] and Fredricks et al. [1971]. Although the original identification of the plasma wave mode was somewhat uncertain, subsequent studies by various investigators, including Gurnett and Frank [1975], Filbert and Kellogg [1979] and Anderson et al. [1981], confirmed that the waves are electrostatic electron plasma oscillations (also called Langmuir waves). The $\vec{k}$ vector of these waves is aligned along the static magnetic field, as would be expected if they are excited by electrons streaming along the magnetic field.

The electron plasma oscillations are usually most intense near the foreshock boundary and become weaker and more irregular in the region behind the boundary (see Figure 11). Typical electric field intensities range from a few hundred μVm^{-1} to about ten mVm^{-1}. The spectrum of the electron plasma oscillations is highly variable. Near the foreshock boundary the emission usually occur in a narrow frequency band ($\Delta f/f \sim$ few percent) centered on the electron plasma frequency. However, as the spacecraft moves downstream of the boundary the spectrum spreads both upward and downward in frequency [Etcheto and Faucheux, 1984; Fuselier et al., 1984]. This change in the spectrum is illustrated in Figure 12 [from Fuselier et al., 1984], which shows an electric field spectrogram (A) near the foreshock boundary, and another (B) farther downstream. As can be seen the spectrum deep in the foreshock becomes very complex. At Jupiter the electric field waveform of electron plasma oscillations in the foreshock has been shown to break up into highly structured packets lasting only a few milliseconds [Gurnett et al., 1981a]. An example of these highly structured waveforms is shown in Figure 13. When translated into spatial scale lengths these wave packets are estimated to have dimensions of only a few tens of Debye lengths.

Gurnett et al. have suggested that these wave packets may be envelope solitons that have collapsed down to spatial scales of only a few Debye lengths.

Several other types of plasma waves are also association with strong electron plasma oscillations, apparently due to other nonlinear effects. An example of one of these nonlinear effects can be seen in Figure 11 from about 1909 to 1913 UT. During this time a broadband enhancement can be seen below about 1 kHz that is coincident with the intense burst of plasma oscillations in the 56.2 kHz channel. These low-frequency electric field enhancements were noted by Anderson et al. [1981], who suggest that they may be ion acoustic waves excited by nonlinear coupling to the electron plasma oscillations. Kennel et al. [1980] and Anderson et al. [1981] have also reported electromagnetic whistler-mode emissions that are closely correlated with intense bursts of electron plasma oscillations. Electromagnetic emissions at twice the electron plasma frequency, $2f_p$, are also known to be generated in the upstream region and have been described by Gurnett and Frank [1975], and Hoang et al. [1981]. It is widely believed that these $2f_p$ electromagnetic emissions are produced by mode coupling to electron plasma oscillations, similar to the mechanisms thought to be responsible for Type II and Type IV solar radio bursts [Kundu, 1965].

In addition to the electron plasma oscillations, low frequency hydromagnetic waves with frequencies near 1 Hz are also observed in the electron foreshock [Hoppe et al., 1982]. Although originally reported in association with upstream ion beams it now appears certain that the waves are actually associated with the electron foreshock [Sentman et al., 1983]. Measurements of the phase velocity and polarization of these waves have been

performed by Hoppe et al. [1982] using data from the ISEE-1 and -2 spacecraft. These measurements show that although the waves are left-hand polarized with respect to the static magnetic field in the spacecraft frame of reference, in the plasma rest frame the waves are actually right-hand polarized. The polarization reversal between the two frames of reference occurs because the phase velocity is less than the solar wind velocity. For wave vectors directed toward the sun the waves are carried downstream by the motion of the solar wind, thereby reversing the sense of polarization. The wave frequency in the rest frame is typically 20 to 100 times the proton cyclotron frequency. This combination of polarization and frequency uniquely identifies the waves as whistler mode emissions.

After entering the electron foreshock the spacecraft may or may not encounter the ion foreshock. The ion foreshock only exists in the region where the shock is quasi-parallel, because ions can only escape into the upstream region if $\theta_{Bn} \gtrsim 45°$. For quasi-parallel shocks the ion foreshock boundary is almost always associated with the onset of strong electrostatic noise in the frequency range from a few hundred Hz to about 10 kHz and intense ULF (ultra-low-frequency) magnetohydrodynamic waves. The shock in Figure 11 is a quasi-parallel shock and has a well-defined ion foreshock region [personal communication, G. Parks]. The entry into the ion foreshock in this case can be easily identified by the onset of the strong electrostatic noise from about 100 Hz to 10 kHz at about 1937 UT. This type of electrostatic noise and its association with energetic, 1 to 40 keV, ions streaming into the solar wind ahead of the shock were first reported by Scarf et al. [1971]. Until relatively recently the identification of the mode of propagation of this noise has been somewhat controversial. The

difficulty is the same as for the high frequency electrostatic noise in the transition region. If the wavelengths are very short then the Doppler shift is so large that the mode of propagation can not be uniquely identified on the basis of the frequency spectrum alone. Gurnett and Frank [1978] initially suggested that this noise could be accounted for by Doppler-shifted ion-acoustic waves. Other modes have also been suggested, such as the Buneman mode [Rodriguez, 1981], and an ion-beam mode [Lemons et al., 1979]. Recently Fuselier and Gurnett [1984], using interferometry techniques, have been able to measure the wavelength of the waves. These measurements show, with very little doubt, that the waves are ion-acoustic waves.

Typically, the ion-acoustic waves observed in the ion foreshock have electric field strengths ranging from a few tens of μV/m to about one mV/m. Although the ion-acoustic waves appear to have a broad bandwidth in multichannel plots such as in Figure 11, in fact the bandwidth is quite narrow. The narrow bandwidth of the emission can be seen in high resolution spectrograms of the type shown in Figure 14. As this illustration shows, the emission occurs in a single narrow emission that fluctuates rapidly in frequency from a few hundred Hz to about ten kHz. The rapid frequency variations give the appearance of a broad bandwidth in the multichannel plots. Because the frequency is determined by the Doppler shift, these frequency variations are mainly due to variations in the wavelength of the ion-acoustic wave. To a good approximation the upper frequency limit of the waves is given by $V_{sw}/2\pi\lambda_D$.

Waves nearly identical to the ion-acoustic waves observed upstream of the earth's bow shock have also been observed upstream of the bow shock at Jupiter [Scarf et al., 1979], at Saturn [Gurnett et al., 1981b], and

upstream of interplanetary shocks [Kennel et al., 1982]. In the case of interplanetary shocks it has been shown that the ion-acoustic noise is only observed for quasi-parallel shocks with $\theta_{Bn} \lesssim 45°$ [Kennel et al., 1982]. This result is consistent with the terrestrial observations which show that the ion acoustic noise only occurs ahead of quasi-parallel shocks. Although it seems likely that the ion-acoustic waves observed ahead of interplanetary shocks are caused by ions streaming out ahead of the shock, to date there has been no conclusive identification of these ions.

In addition to the ion-acoustic waves, the ion foreshock is also filled with intense ULF magnetohydrodynamic waves with frequencies of about 0.03 Hz. The ULF waves were first discussed in detail by Greenstadt et al. [1968] and Fairfield et al. [1969]. These waves are often very intense, with magnetic field amplitudes often comparable to the solar wind magnetic field strength. A typical plot of the magnetic field amplitude of the ULF waves is shown in Figure 15 [from Fairfield et al., 1969]. As can be seen the waves are quite coherent, often consisting of nearly monochromatic wave packets lasting several minutes or longer. Measurements of the phase velocity and polarization of these waves have been carried out by Hoppe and Russell [1983] using data from the ISEE-1 and -2 spacecraft. These measurements show that although the wave polarization is left-hand in the spacecraft rest frame, the polarization is actually right-hand in the plasma rest frame. This polarization reversal between the two frames of reference occurs because the phase velocity is less than the solar wind velocity, very similar to the situation with the 1 Hz waves. The rest frame frequency of the ULF waves is typically about one-tenth of the proton cyclotron frequency. The polarization and frequency measurements clearly show that the

ULF waves are propagating in the right-hand polarized magnetosonic mode (low frequency magnetohydrodynamic limit of the whistler mode). These waves often show evidence of nonlinear effects, with a tendency to steepen into sawtooth-like waveforms and to form soliton-like wave packets.

A. Interpretation of the Upstream Electron Plasma Oscillations

For many years it has been widely accepted that an electron beam-plasma instability is responsible for the upstream electron plasma oscillations. This mechanism was originally proposed by Fredricks et al. [1971]. Despite the early agreement on the origin of the instability it has been difficult to verify that the reduced one-dimensional distribution function actually has the region of positive slope, $\partial F/\partial v_{\parallel} > 0$, required by the theory [see Krall and Trivelpiece, 1973]. Using electron measurements from IMP-8 Gurnett and Frank [1975] showed that the electron plasma oscillations were associated with a well-defined peak in the electron distribution function at an energy of a few hundred eV. However, they did not show that the reduced one-dimensional distribution function had a region of positive slope. It has only been very recently that Klimas [1983], using electron measurements from ISEE-1, actually demonstrated that a region of positive slope (i.e., a beam) is present during a period when electron plasma oscillations are being observed.

The issues that remain to be resolved concerning the upstream electron plasma oscillations mainly involve nonlinear effects. A long standing problem in all beam-plasma interactions is to explain how the beam can propagate long distances without being disrupted by the electrostatic waves. It is widely believed that some nonlinear mechanism must act to limit the wave amplitudes and/or take the wave out of resonance with the beam. For a

review of some of the mechanisms that have been proposed, see Papadopoulos [1978]. Since electron plasma oscillations are observed to propagate at least 200 R_E from the earth, it is clear that some mechanism must be stabilizing the beam. The complex amplitude and frequency structure of the electron plasma observed upstream of the earth (Figure 12) and Jupiter (Figure 13) probably provide important clues to the mechanisms involved. However, a full understanding of these beam stabilization effects will require considerable further study.

B. Interpretation of the Upstream Ion Acoustic Waves

Although it is known that the upstream ion acoustic waves are produced by energetic, ~ 1 to 40 keV, ions streaming into the solar wind, the detailed mechanism responsible for these waves remains unknown. The most obvious possibility is that the waves are produced by an ion beam instability. However, this simple explanation encounters serious difficulties. First, as discussed by Lemons et al. [1979] a beam-driven ion-acoustic instability typically requires $T_e/T_i \gtrsim 5$. Although this requirement is sometimes satisfied, in many cases ion acoustic waves are observed when this condition is not satisfied. Second, computer studies of the electrostatic dispersion relation [personal communication, S. Fuselier] show that the ion beam temperature must be quite low for an ion beam-driven instability to occur, usually less than the solar wind ion temperature. Most studies of the upstream ion distribution [Paschmann et al., 1981; Eastman et al., 1981] indicate that the temperatures of the upstream ions are too high for an ion-beam instability to occur. However, it is possible that the ion beam temperatures may be overestimated. Recently, Eastman et al. [1981] and

Gurgiolo et al. [1981] have reported evidence of gyro-phase bunching effects in the upstream ion distributions. These observations suggest that fine structure may exist in the upstream ion distributions and that the temperature of this fine structure may be much lower than the average temperature of the entire distribution. A full analysis of these effects will require plasma instrumentation with much better temporal and angular resolution than is currently available.

Because of the difficulties with the ion-beam mechanism another ion-acoustic instability mechanism has been proposed by Gurnett and Frank [1978]. This mechanism is based on a return current induced by the upstream ions beams. Because the upstream ions carry charge away from the shock, this charge imbalance must be compensated by a return current. This return current must be carried by a relative drift between the solar wind electrons and ions. Calculations of the drift velocity show that it is close to the ion-acoustic threshold if the electron to ion temperature ratio is sufficiently large $T_e/T_i \gg 1$. However, the instability cannot occur it $T_e/T_i \lesssim 1$. Thus, although promising, the return current mechanism has the same difficulty with the T_e/T_i ratio that occurs in the ion-beam instability.

C. Interpretation of the Upstream Magnetohydrodynamic Waves

Two types of low frequency magnetohydrodynamic waves must be considered: (1) the waves with frequencies near 1 Hz, and (2) the ULF waves with frequencies near 0.03 Hz. Both types of waves are right-hand polarized in the plasma rest frame and are propagating in the whistler mode. In the case

of the 1 Hz waves the frequency is above the proton cyclotron frequency, and in the case of the 0.03 Hz waves is below the proton cyclotron frequency. Because both waves are propagating in essentially the same mode, the difference in characteristics must be due to the mechanism by which the waves are excited. For the 1 Hz waves Sentman et al. [1983] have investigated an anisotropy in the upstream electron distribution as the free energy source, and for the 0.03 Hz ULF waves Gary et al. [1981] and Sentman et al. [1981] have investigated various interactions with the upstream ion distributions (both beams and diffuse ions) as the free energy source. The anisotropy in the upstream electron distribution appears to be an adequate free energy source for the 1 Hz waves. In the case of the ULF waves the main uncertainties involve the relative importance of the beam and diffuse ion distributions. Both ion distributions are present in the ion foreshock region and both distributions can cause wave growth in the correct frequency range. The problem is complicated by the fact that once generated, the waves can be convected from the region where ion beams are observed into the region where the diffuse ion distributions occur. One interesting possibility is that the waves may be responsible for the diffuse ion distribution. This possibility has been suggested by Winske and Leroy [1984] and has been supported by computer simulations that show the ions being diffused into a ring-shaped region in velocity space by an electromagnetic ion beam instability.

IV. THE DOWNSTREAM REGION

Inspection of typical shock crossings, such as in Figure 1, shows that although the highest intensities occur in the transition region, substantial wave intensities continue for long distances downstream of the shock. For the earth's bow shock the downstream noise extends throughout the entire region between the shock and the magnetopause, a distance of several earth radii or more. For interplanetary shocks the downstream noise sometimes persists for several hours, corresponding to downstream distances as large as 0.1 A.U.

Two types of noise can be identified in the downstream region: electrostatic and electromagnetic. Rodriguez identified three components in the downstream electrostatic noise: (1) a low frequency component below a few hundred Hz, (2) a high frequency component with a peak intensity near a about one kHz, and (3) a weak narrowband component near the electron plasma frequency. The low and high frequency components have spectrums very similar to the low and high frequency components of the electric field noise observed in the transition region. Usually the low frequency component decays rapidly downstream of the shock (as in Figure 1), leaving the high frequency component as the dominant type of electrostatic noise downstream of the shock. The spectrum of this noise is very similar to the ion-acoustic wave observed upstream of the shock. Rodriguez [1979] has shown that the electric field of the high frequency noise is aligned parallel to

the static magnetic field. The narrowband component almost certainly consists of electron plasma oscillations, since the center frequency is close to the electron plasma frequency. The electron plasma oscillations in the downstream region are usually very weak, much weaker than in the upstream region.

The electromagnetic noise in the downstream region consists of a weak but persistent broadband component at frequencies below a few hundred Hz [Smith et al., 1967], and very intense narrowband emissions near 100 Hz [Smith et al., 1969]. These latter emissions are called lion roars because, when played into a speaker, they sound like a lion's roar. Lion roars are responsible for the brief impulsive bursts in the 31.1 and 56.2 Hz channels of Figure 1, downstream of the shock. The peak magnetic field strengths of the lion roars are rather large, typically in the range from about 40 to 160 pT. Polarization measurements by Smith and Tsurutani [1976] show that the lion roars are propagating in the right-hand polarized whistler mode.

A. Interpretation of the Downstream Electrostatic Noise

The origin of the electrostatic noise observed downstream of the shock has received virtually no attention. Since the noise extends continuously downstream of the shock and has a spectrum similar to the electrostatic noise in the transition region, it seems likely that the noise consists of waves that are simply convected downstream from the transition region. The best evidence of a transition region source comes from interplanetary shocks. In some cases, interplanetary shocks show an exponential decay of the electrostatic wave intensities with increasing distance behind the shock

[Gurnett et al., 1979]. An exponential intensity variation suggests that the waves are undergoing simple linear damping as they are carried downstream of the shock. It is hard to imagine a local generation mechanism that would give a simple exponential decay. The main difficulty with this simple wave transport picture is that the electrostatic waves are often present for many tens of minutes after the shock crossing. Such a long persistence time implies an extraordinarily low damping rate, $\gamma/\omega \sim 10^{-5}$ to 10^{-6} for ion-acoustic waves. How the plasma could achieve and maintain a state with such a low damping is not known. Another puzzling observation is that at Jupiter and Saturn the electrostatic noise decays very rapidly downstream of the shock, much quicker than behind the earth's bow shock.

B. Interpretation of the Downstream Electromagnetic Noise

The origin of the broadband low frequency component of the electromagnetic noise has received very little attention. Smith et al. [1967] suggested that this noise is probably caused by whistler mode waves. If the broadband component is due to whistler mode waves then the waves could either be generated in the transition region, or they could be generated locally. For interplanetary shocks the intensity of the broadband magnetic noise is sometimes observed to decrease exponentially with increasing distance from the shock [Gurnett et at., 1979; Kennel et al., 1982]. These observations suggest that the noise is generated in the transition region and slowly damps as it propagates into the downstream region. Again, it seems unlikely that such an exponential decay could be accounted for by a local generation mechanism.

The origin of the lion roar emissions has been discussed by several investigators, including Smith et al. [1969], Smith and Tsurutani [1976], Thorne and Tsurutani [1981], and Tsurutani et al. [1982]. For these emissions it is almost certain that the waves are generated locally since the emissions are closely correlated with local depressions in the magnetic field. As currently understood, it is believed that the lion roars are produced by an electron cyclotron resonance instability that occurs when the electrons have a $T_\perp > T_\parallel$ anisotropy. Typical energies for electron cyclotron resonance interaction with these waves are about 10 to 30 eV. Usually the cyclotron resonance energy is above the thermal energy of the electrons. However, when the magnetic field strength is depressed the resonance energy drops down into the thermal distribution, thereby greatly enhancing the whistler-mode growth rates if the appropriate, $T_\perp > T_\parallel$, anisotropy is present. Typical electron anisotropies, $T_\perp/T_\parallel$, in the region downstream of the shock range from about 1.06 to 1.2 [Tsurutani et al., 1982]. For these anisotropies the whistler-mode growth rates are estimated to be about 100 db/R_E [Thorne and Tsurutani, 1981]. These growth rates are more than adequate to explain the observed lion roar intensities.

V. CONCLUSIONS

In this review we have described the waves and instabilities that occur at collisionless shocks and commented on the mechanisms responsible for the generation of these waves. It is obvious that although considerable progress has been made, there are still many unanswered questions concerning the origin of these waves and instabilities. In closing this review we wish to comment on the areas in which further advances can be made, either by improvements in the instrumentation, or by better and more complete analysis of existing data.

As has been described, the interpretation of the wave observations is often complicated by the fact that the plasma is streaming by the spacecraft at a high speed, thereby introducing a large and usually unknown Doppler shift. This problem is particularly serious for electrostatic waves, which usually have short wavelengths. The proper interpretation of the Doppler shift requires knowledge of the wavelength and direction of propagation of the wave. Various possibilities exist for obtaining improved information on the Doppler shift. Because large directional antenna arrays with dimensions of many wavelengths (hundreds of meters) are probably not feasible, the only known technique is to use the antenna as an interferometer, as has been done by Fuselier and Gurnett [1974]. This technique can be improved by using longer antennas (the longest wavelength that can be resolved is limited by the length of the antenna) and antennas of differnent lengths (to provide

simultaneous measurements at several wavelengths). Phase measurements between various antenna elements, such as has recently been demonstrated by Kintner et al. [1984], can also give improved information on the wavelength and phase velocity of the waves.

To resolve beams and other nonthermal features that act as free energy sources for waves much better measurements of the plasma distribution function are required. Improved temporal resolution and better 3-d velocity space coverage would be particularly helpful in determining if the upstream ion distributions have a cold beam component that could be responsible for the upstream ion-acoustic waves. Improved temporal and velocity space resolution would also help identify the features responsible for the fine structure in the upstream electron plasma oscillations.

Last, but not least, it should be emphasized that significant advances can still be made by improved analysis and modelling of existing data. More work needs to be done using measured particle distribution functions to compute the growth rate and frequency of unstable modes. In such calculations special care must be taken to fully understand the instrumental effects on the measured particle distribution functions. In many cases beams or other small features may exist that are not resolved in the existing data. In cases where adequate resolution is not available, plasma simulations may provide important clues indicating which sources of free energy are most important. More work also needs to be done on shock simulation codes that can adequately model turbulent dissipation processes, especially those that operate on spatial scales comparable to the Debye length.

ACKNOWLEDGEMENTS

This research has been supported by NASA through contract NAS5-26819 with Goddard Space Flight Center, grants NGL-16-001-002 and NGL-16-001-043 with NASA Headquarters, and contract N00014-76-C-0016 with the Office of Naval Research.

REFERENCES

Anderson, R. R., G. K. Parks, T. E. Eastman, D. A. Gurnett, and L. A. Frank, Plasma waves associated with energetic particles streaming into the solar wind from the earth's bow shock, J. Geophys. Res., 86, 4493, 1981.

Buneman, O., Instability, turbulence, and conductivity in current-carrying plasma, Phys. Rev. Lett., 1, 8, 1958.

Coroniti, F. V., C. F. Kennel, F. L. Scarf, and E. J. Smith, Whistler mode turbulence in the disturbed solar wind, J. Geophys. Res., 87, 6029, 1982.

Davidson, R. C., and N. T. Gladd, Anomalous transport properties associated with the lower-hybrid-drift instability, Phys. Fluids, 18, 1327, 1975.

Dum, C. T., E. Marsch, and W. Pilipp, Determination of wave growth from measured distribution functions and transport theory, J. Plasma Phys., 23, 91, 1980.

Eastman, T. E., R. R. Anderson, L. A. Frank, and G. K. Parks, Upstream particles observed in the earth's foreshock region, J. Geophys. Res., 86, 4379, 1981.

Etcheto, J., and M. Faucheux, Detailed study of electron plasma waves upstream of the Earth's bow shock, J. Geophys. Res., 89, 6631, 1984.

Fairfield, D. H., Bow shock associated waves observed in the far upstream interplanetary medium, J. Geophys. Res., 74, 3541, 1969.

Feldman, W. C., S. J. Bame, S. P. Gary, J. T. Gosling, D. McComas, M. F. Thomsen, G. Paschmann, N. Sckopke, M. M. Hoppe, and C. T. Russell, Electron heating within the earth's bow shock, Phys. Rev. Lett., 49, 199, 1982.

Filbert, P. C., and P. J. Kellogg, Electrostatic noise at the plasma frequency beyond the bow shock, J. Geophys. Res., 84, 1369, 1979.

Fredricks, R. W., G. M. Crook, C. F. Kennel, I. M. Green, F. L. Scarf, P. J. Coleman, and C. T. Russell, OGO 5 observations of electrostatic turbulence in bow shock magnetic structures, J. Geophys. Res., 75, 3751, 1970.

Fredricks, R. W., C. F. Kennel, F. L. Scarf, G. M. Crook, and I. M. Green, Detection of electric field turbulence in the earth's bow shock, Phys. Rev. Lett., 21, 1761, 1968.

Fredricks, R. W., F. L. Scarf, and L. A. Frank, Nonthermal electrons and high frequency waves in the upstream solar wind, 2, Analysis and interpretation, J. Geophys. Res., 76, 6691, 1971.

Fuselier, S. A., and D. A. Gurnett, Short wavelength ion waves upstream of the earth's bow shock, J. Geophys. Res., 89, 91, 1984.

Fuselier, S. A., D. A. Gurnett, and R. J. Fitzenreiter, Downshifts of electron plasma oscillations in the foreshock region, J. Geophys. Res., in preparation, 1984.

Gary, S. P., Ion-acoustic-like instabilities in the solar wind, J. Geophys. Res., 83, 2504, 1978.

Gary, S. P., J. T. Gosling, and D. W. Forslund, The electromagnetic ion beam instability upstream of the earth's bow shock, J. Geophys. Res., 86, 6691, 1981.

Gosling, J. T., J. R. Asbridge, S. J. Bame, G. Paschmann, and N. Sckopke, Observations of two distinct populations of bow shock ions in the upstream solar wind, Geophys. Res. Lett., 5, 957, 1978.

Greenstadt, E. W., and R. W. Fredricks, Shock systems in collisionless space plasmas, Solar System Plasma Physics, Vol. III., ed. by L. J. Lanzerotti, C. F. Kennel, and E. N. Parker, North-Holland Publishing Co., Amsterdam, 3, 1979.

Greenstadt, E. W., I. M. Green, G. T. Inouye, A. J. Hundhausen, S. J. Bame, and I. B. Strong, Correlated magnetic field and plasma observations of the earth's bow shock, J. Geophys. Res., 73, 51, 1968.

Gurgiolo, C., G. K. Parks, B. H. Mauk, C. S. Lin, K. A. Anderson, R. P. Lin, and H. Reme, Non-$\vec{E}\times\vec{B}$ ordered ion beams upstream of the earth's bow shock, J. Geophys. Res., 86, 4415, 1981.

Gurnett, D. A., and L. A. Frank, Electron plasma oscillations associated with type III radio emissions and solar electrons, Solar Phys., 45, 477, 1975.

Gurnett, D. A., and L. A. Frank, Ion acoustic waves in the solar wind, J. Geophys. Res., 83, 58, 1978.

Gurnett, D. A., W. S. Kurth, and F. L. Scarf, Plasma waves near Saturn: Initial results from Voyager 1, Science, 212, 235, 1981b.

Gurnett, D. A., J. E. Maggs, D. L. Gallagher, W. S. Kurth, and F. L. Scarf, Parametric interaction and spatial collapse of beam-driven Langmuir waves in the solar wind, J. Geophys. Res., 86, 8833, 1981a.

Gurnett, D. A., F. M. Neubauer, and R. Schwenn, Plasma wave turbulence associated with interplanetary shocks, J. Geophys. Res., 84, 541, 1979.

Hoang, S., J. Fainberg, and J. L. Steinberg, The $2f_p$ circumterrestrial radio emission as seen from ISEE 3, J. Geophys. Res., 86, 4531, 1981.

Holzer, R. E., M. G. McLeod, and E. J. Smith, Preliminary results from the OGO 1 search coil magnetometer: Boundary positions and magnetic noise spectrum, J. Geophys. Res., 71, 1481, 1966.

Hoppe, M. M., and C. T. Russell, Plasma rest frame frequencies and polarizations of the low-frequency upstream waves: ISEE 1 and 2 observations, J. Geophys. Res., 88, 2021, 1983.

Hoppe, M. M., C. T. Russell, T. E. Eastman, and L. A. Frank, Characteristics of the ULF waves associated with upstream ion beams, J. Geophys. Res., 87, 643, 1982.

Hsia, J. B., S. M. Chiu, M. F. Hsia, R. L. Chou, and C. S. Wu, Generalized lower-hybrid-drift instability, Phys. Fluids, 22, 1737, 1979.

Huba, J. D., and C. S. Wu, Effects of a magnetic field gradient on the lower hybrid drift instability, Phys. Fluids, 19, 988, 1976.

Hundhausen, A. J., Solar Wind and Coronal Expansion, Springer Verlag, N. York, 1972.

Kennel, C. F., F. L. Scarf, F. V. Coroniti, R. W. Fredricks, D. A. Gurnett, and E. J. Smith, Correlated whistler and electron plasma oscillation bursts detected on ISEE-3, Geophys. Res. Lett., 7, 129, 1980.

Kennel, C. F., F. L. Scarf, F. V. Coroniti, E. J. Smith, and D. A. Gurnett, Nonlocal plasma wave turbulence associated with interplanetary shocks, J. Geophys. Res., 87, 17, 1982.

Kintner, P., J. LaBelle, M. C. Kelley, L. J. Cahill, Jr., T. Moore, and R. Arnoldy, Interferometric phase velocity measurements, Geophys. Res. Lett., 11, 19, 1984.

Klimas, A. J., A mechanism for plasma waves at the harmonics of the plasma frequency in the electron foreshock boundary, J. Geophys. Res., 88, 9081, 1983.

Krall, N. A., and A. W. Trivelpiece, Principles of Plasma Physics, McGraw-Hill, N. York, 1973.

Kundu, M., Solar Radio Astronomy, Interscience, N. York, 1965.

Lemons, D. S., J. R. Asbridge, S. J. Bame, W. C. Feldman, S. P. Gary, and J. T. Gosling, The source of electrostatic fluctuations in the solar wind, J. Geophys. Res., 84, 2135, 1979.

McBride, J. B., E. Ott, J. P. Boris and J. H. Orens, Theory and simulation of turbulent heating by the modified two-stream instability, Phys. Fluids, 15, 2367, 1972.

Ness, N. F., C. S. Searce, and H. B. Seek, Initial results of the IMP 1 magnetic field experiment, J. Geophys. Res., 69, 3531, 1964.

Neubauer, F. M., G. Musmann, and G. Dehmel, Fast magnetic fluctuations in the solar wind: Helios 1, J. Geophys. Res., 82, 3201, 1977.

Olsen, J. V., R. E. Holzer, and E. J. Smith, High-frequency magnetic fluctuations associated with the earth's bow shock, J. Geophys. Res., 74, 4601, 1969.

Papadopoulos, K., On the physics of strong turbulence for electron plasma waves, Proceedings of the Varenna School of Plasma Physics, Pergamon Press, N. York, 355, 1978.

Paschmann, G., N. Sckopke, S. J. Bame, and J. T. Gosling, Observations of gyrating ions in the foot of the nearly perpendicular bow shock, Geophys. Res. Lett., 9, 881, 1982.

Paschmann, G., N. Sckopke, I. Papamastorakis, J. R. Asbridge, S. J. Bame, and T. Gosling, Characteristics of reflected and diffuse ions upstream from the earth's bow shock, J. Geophys. Res., 86, 4355, 1981.

Paul, J. W. M., L. S. Holmes, M. J. Parkinson, and J. Sheffield, Experimental observations on the structure of collisionless shock waves in a magnetized plasma, Nature, 208, 133, 1965.

Priest, E. R., and J. J. Sanderson, Ion acoustic instability in collisionless shocks, Plasma Phys., 14, 951, 1972.

Rodriguez, P., Magnetosheath electrostatic turbulence, J. Geophys. Res., 84, 917, 1979.

Rodriguez, P., Ion waves associated with solar and beam-plasma interactions, J. Geophys. Res., 86, 1279, 1981.

Rodriguez, P., and D. A. Gurnett, Electrostatic and electromagnetic turbulence associated with the earth's bow shock, J. Geophys. Res., 80, 19, 1975.

Rodriguez, P., and D. A. Gurnett, Correlation of bow shock plasma wave turbulence with solar wind parameters, J. Geophys. Res., 81, 2871, 1976.

Scarf, F. L., Wave-particle phenomena associated with shocks in the solar wind, Proceedings of the De Feiter Memorial Symposium on the Study of Traveling Interplanetary Phenomena, D. Reidel, Hingham, Mass., 1978.

Scarf, F. L., D. A. Gurnett, and W. S. Kurth, Jupiter plasma wave observations: An initial Voyager 1 overview, Science, 204, 991, 1979.

Scarf, F. L., R. W. Fredricks, L. A. Frank, and M. Neugebauer, Nonthermal electrons and high-frequency waves in the upstream solar wind, 1, Observations, J. Geophys. Res., 76, 5162, 1971.

Scarf, F. L., R. W. Fredricks, I. M. Green, and G. M. Crook, Observations of interplanetary plasma waves, spacecraft noise, and sheath phenomena on IMP 7, J. Geophys. Res., 79, 73, 1974.

Scarf, F. L., D. A. Gurnett, and W. S. Kurth, Plasma wave turbulence at planetary bow shocks, Nature, 292, 747, 1981.

Scarf, F. L., W. W. L. Taylor, C. T. Russell, and R. C. Elphic, Pioneer Venus plasma wave observations: The solar wind Venus interaction, J. Geophys. Res., 85, 7599, 1980.

Sentman, D. D., J. P. Edmiston, and L. A. Frank, Instabilities of low frequency parallel propagating electromagnetic waves in the earth's foreshock region, J. Geophys. Res., 86, 7487, 1981.

Sentman, D. D., M. F. Thomsen, S. Peter Gary, W. C. Feldman, and M. M. Hoppe, The oblique whistler instability in the earth's foreshock, J. Geophys. Res., 88, 2048, 1983.

Smith E. J., R. E. Holzer, M. G. McLeod, and C. T. Russell, Magnetic noise in the magnetosheath in the frequency range 3-300 Hz, J. Geophys. Res., 72, 4803, 1967.

Smith, E. J., R. E. Holzer, and C. T. Russell, Magnetic emissions in the magnetosheath at frequencies near 100 Hz, J. Geophys. Res., 74, 3027, 1969.

Smith, E. J., and B. T. Tsurutani, Magnetosheath lion roars, J. Geophys. Res., 81, 2261, 1976.

Stix, T. H., The Theory of Plasma Waves, McGraw-Hill, N. York, 1962.

Thomsen, M. F., H. C. Barr, S. Peter Gary, W. C. Feldman, and T. E. Cole, Stability of electron distributions within the Earth's bow shock, J. Geophys. Res., 88, 3035, 1983.

Thorne, R. M., and B. T. Tsurutani, Generation of magnetosheath lion roars, Nature, 293, 384, 1981.

Tidman, D. A., and N. A. Krall, Shock Waves in Collisionless Plasmas, Wiley, N. York, 1971.

Tokar, R. L., D. A. Gurnett, and W. C. Feldman, Whistler mode turbulence generated by electron beams in Earth's bow shock, J. Geophys. Res., 89, 105, 1984.

Tsurutani, B. T., E. J. Smith, R. R. Anderson, K. W. Ogilvie, J. D. Scudder, D. N. Baker, and S. J. Bame, Lion roars and nonoscillatory drift mirror waves in the magnetosheath, J. Geophys. Res., 87, 6060, 1982.

Vaisberg, O. L., A. A. Galeev, G. N. Zastenker, S. I. Klimov, M. N. Nozdrachev, R. Z. Sagdeev, A. Yu. Sokolou, and V. D. Shapiro, Electron acceleration in front of collisionless shock waves, USSR Academy of Sciences, Space Research Institute Report No. 813, 1983.

Winske, D., Microtheory of collisionless shock current layers, to be published in Proceedings of the Chapman Conference on Collisionless Shock Waves in the Heliosphere, Napa Valley, California, 1984.

Winske, D., and M. M. Leroy, Diffuse ions produced by electromagnetic ion beam instabilities, J. Geophys. Res., 89, 2673, 1984.

Wu, C. S., Y. M. Zhou, S. T. Tsai, S. C. Guo, D. Winske, and K. Papadopoulos, A kinetic lower-hybrid cross-field streaming instability, Phys. Fluids, 1982.

FIGURE CAPTIONS

Figure 1 A multichannel electric and magnetic field plot showing typical plasma wave intensities observed near the earth's bow shock.

Figure 2 Measured electric and magnetic field spectrums of plasma waves in the transition region of the earth's bow shock. From Rodriguez and Gurnett [1975].

Figure 3 A schematic representation of electric and magnetic field spectrums observed in the earth's bow shock.

Figure 4 A comparison of the transition region electric field spectrums from four planets: Venus, Earth, Jupiter and Saturn.

Figure 5 Representative electric and magnetic field spectrums for a series of interplanetary shocks observed by ISEE-3 at 1 AU.

Figure 6 A scatter plot showing the variation in the intensity of the high frequency electrostatic noise as a function of the electron to ion temperature ratio. From Rodriguez and Gurnett [1976].

Figure 7 Electric field and plasma measurements of quasi-perpendicular shock from ISEE-1 showing that the onset of the high frequency electrostatic noise occurs coincident with the onset of ions (N_I) gyrating ahead of the shock. Plasma data from Paschmann et al. [1982].

Figure 8 A series of $v_{\parallel}$ cuts of the electron velocity distribution function obtained in the vicinity of the earth's bow shock. Note the beam in the transition region. Plasma data from Feldman et al. [1982].

Figure 9 A spectrum from Prognoz 8 showing a peak in the low frequency electric field noise near the lower hybrid resonance frequency. From Vaisberg et al. [1983].

Figure 10 An illustration showing the geometric relationship between the shock transition region, the tangent field line, and the electron and ion foreshock regions.

Figure 11 A multichannel electric field plot showing the onset of electron plasma oscillations at the electron foreshock and the onset of ion-acoustic waves at the ion foreshock.

Figure 12 High resolution frequency-time spectrograms showing the change in the spectrum of electron plasma oscillations from a very narrowband emission near the electron foreshock boundary (A) to a much broader highly structured emission deep in the foreshock (B). From Fuselier et al. [1984].

Figure 13 Examples of soliton-like structures in the waveform of electron plasma oscillations observed upstream of Jupiter's bow shock. From Gurnett et al. [1981a].

Figure 14 High resolution frequency-time spectrograms of ion-acoustic waves observed in the ion foreshock region of the earth's bow shock. From Anderson et al. [1981].

Figure 15 An example of the magnetic fluctuations associated with the upstream ULF magnetohydrodynamic waves. Note the highly coherent nature of these waves and the large amplitude relative to the background field [from Fairfield, 1969].

TABLE 1

Correlation Coefficient

Upstream Parameter	E_L, Low Frequency Electric Field Noise	E_H, High Frequency Electrostatic Noise	B_L, Magnetic Field Noise
β	-0.29	-0.27	0.15
M_A	-0.29	-0.30	0.15
M_S	0.19	0.24	0.13
$\|B\|$	0.31	0.16	0.34
θ_{Bn}	0.34	0.14	0.39
V_{sw}	-0.16	-0.36	0.30
N	0.03	0.24	0.50
T_e	-0.20	-0.24	-0.12
T_i	-0.38	-0.57	0.18
T_e/T_i	0.42	0.60	-0.11

Here, $\beta = 2\mu_o N\kappa(T_e + T_i)/B^2$, $M_A = V_{sw}/V_A$, and $M_S = V_{sw}/V_S$, where

$V_A = B/\sqrt{\mu_o \rho_m}$, and $V_S = [\frac{5}{3}\kappa(T_e + T_i)/m_i]^{1/2}$.

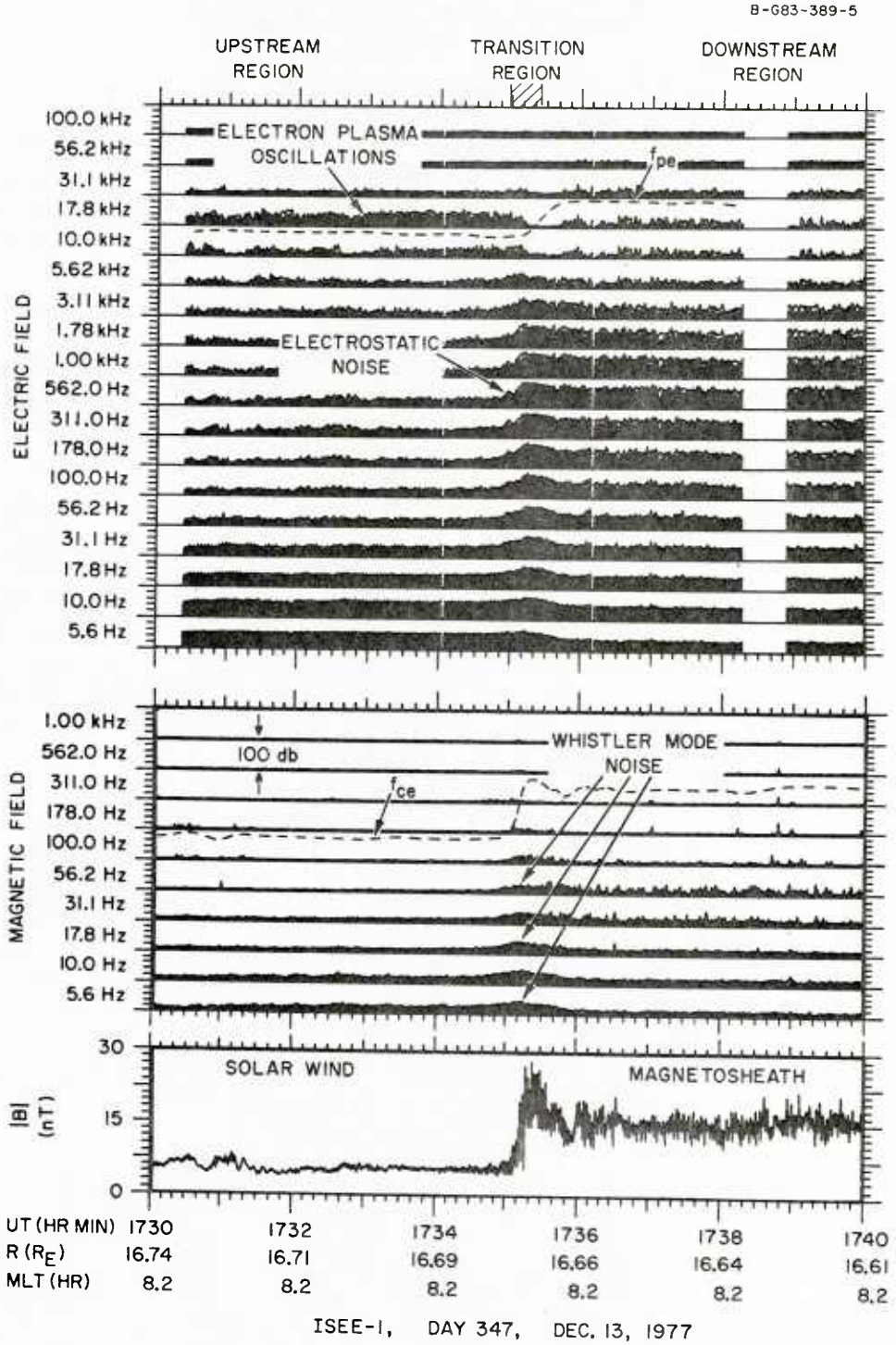
B-G83-389-5
UPSTREAM REGION
TRANSITION REGION
DOWNSTREAM REGION
ELECTRIC FIELD
100.0 kHz
56.2 kHz
31.1 kHz
17.8 kHz
10.0 kHz
5.62 kHz
3.11 kHz
1.78 kHz
1.00 kHz
562.0 Hz
311.0 Hz
178.0 Hz
100.0 Hz
56.2 Hz
31.1 Hz
17.8 Hz
10.0 Hz
5.6 Hz
ELECTRON PLASMA OSCILLATIONS
f_{pe}
ELECTROSTATIC NOISE
MAGNETIC FIELD
1.00 kHz
562.0 Hz
311.0 Hz
178.0 Hz
100.0 Hz
56.2 Hz
31.1 Hz
17.8 Hz
10.0 Hz
5.6 Hz
100 db
f_{ce}
WHISTLER MODE NOISE
|B| (nT)
30
15
0
SOLAR WIND
MAGNETOSHEATH
UT (HR MIN) 1730 1732 1734 1736 1738 1740
R (R_E) 16.74 16.71 16.69 16.66 16.64 16.61
MLT (HR) 8.2 8.2 8.2 8.2 8.2 8.2
ISEE-1, DAY 347, DEC. 13, 1977

Figure 1

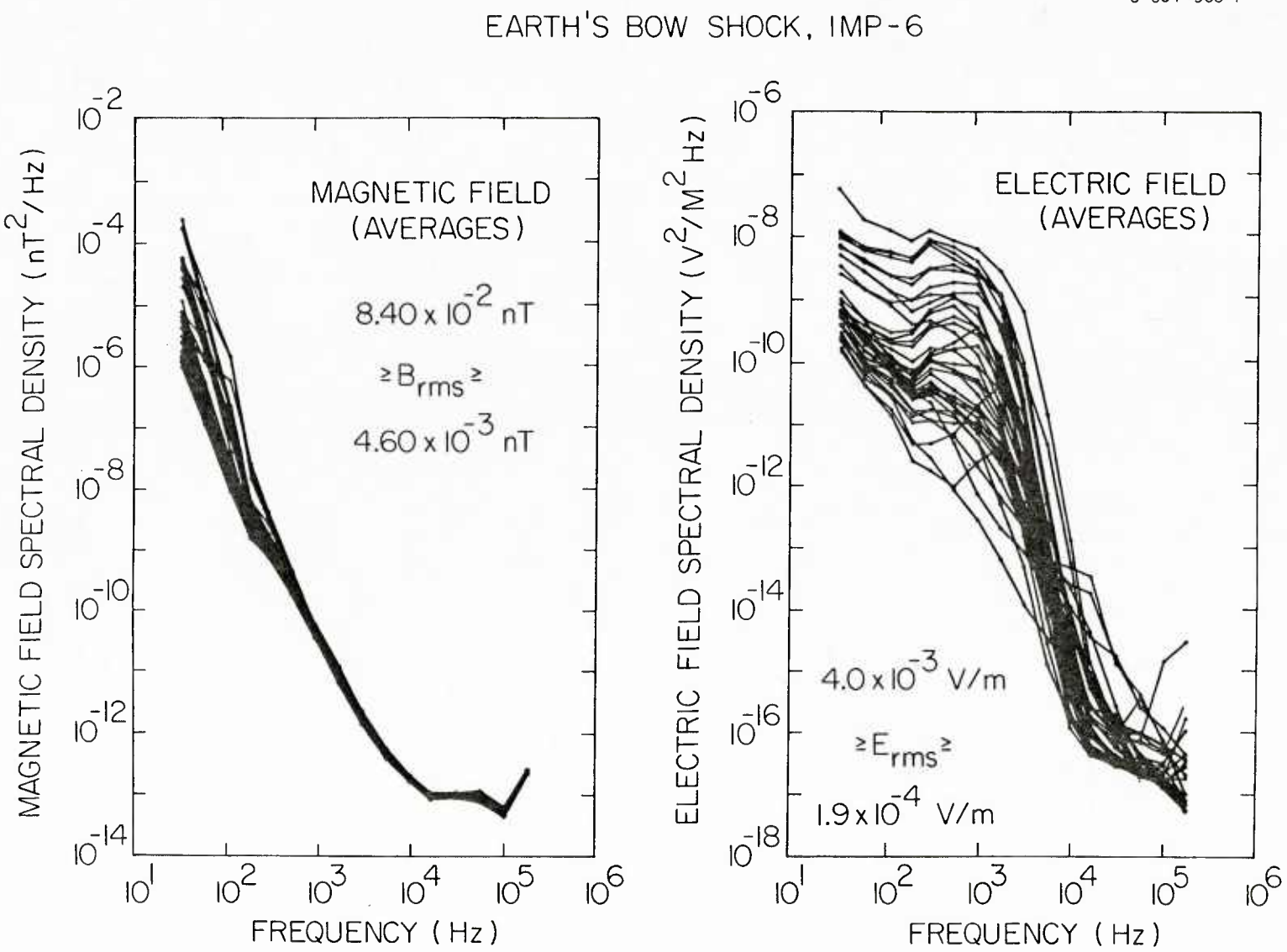
EARTH'S BOW SHOCK, IMP-6
MAGNETIC FIELD SPECTRAL DENSITY (nT²/Hz)
MAGNETIC FIELD
(AVERAGES)
8.40 x 10⁻² nT
≥ B rms ≥
4.60 x 10⁻³ nT
FREQUENCY (Hz)
ELECTRIC FIELD SPECTRAL DENSITY (V²/M² Hz)
ELECTRIC FIELD
(AVERAGES)
4.0 x 10⁻³ V/m
≥ E rms ≥
1.9 x 10⁻⁴ V/m
FREQUENCY (Hz)

Figure 2

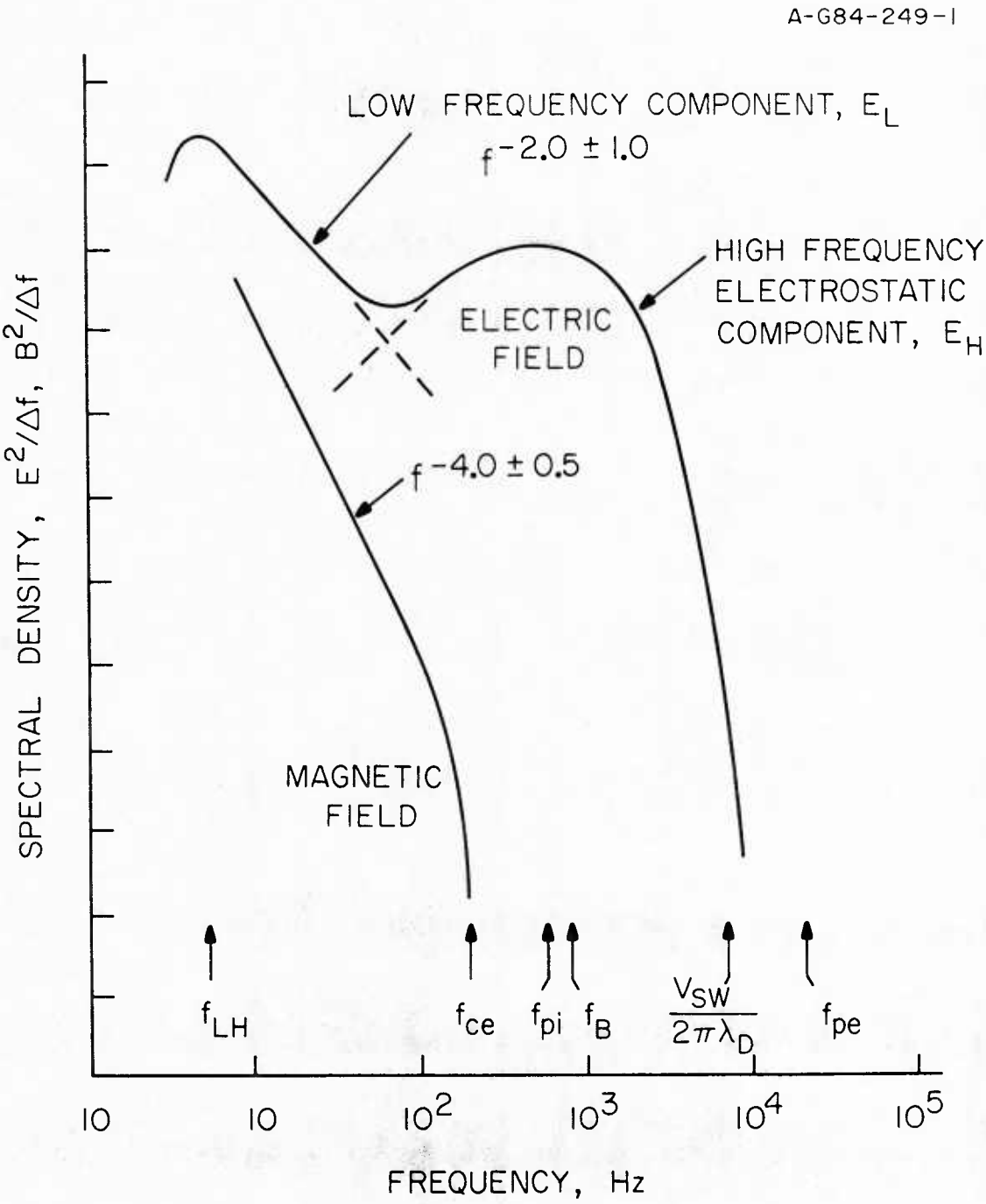
A-G84-249-1
LOW FREQUENCY COMPONENT, E_L
$f^{-2.0 \pm 1.0}$
HIGH FREQUENCY ELECTROSTATIC COMPONENT, E_H
ELECTRIC FIELD
$f^{-4.0 \pm 0.5}$
MAGNETIC FIELD
SPECTRAL DENSITY, $E^2/\Delta f$, $B^2/\Delta f$
f_{LH}
f_{ce}
f_{pi}
f_B
$\frac{V_{SW}}{2\pi\lambda_D}$
f_{pe}
10
10
10^2
10^3
10^4
10^5
FREQUENCY, Hz

Figure 3

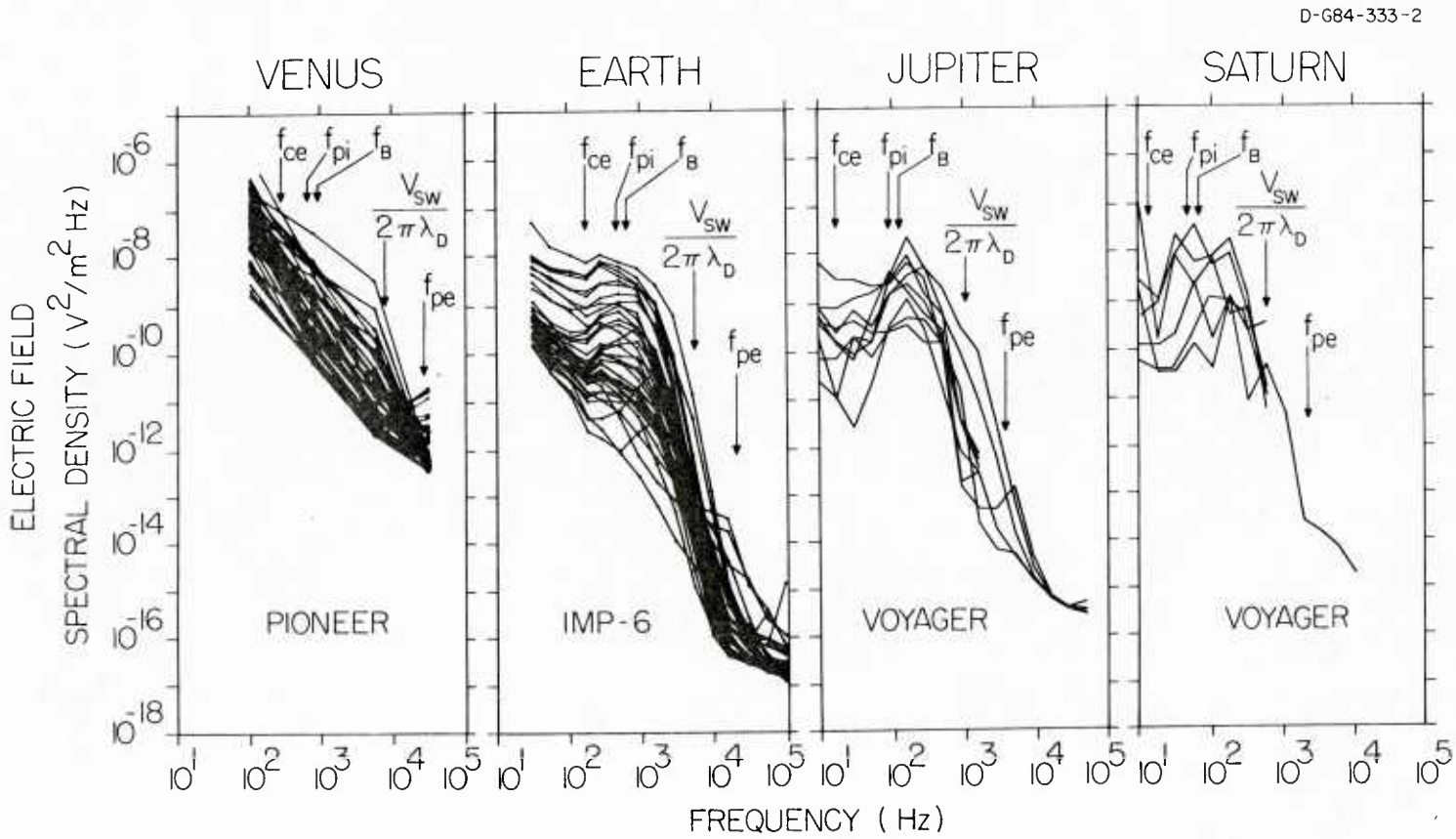
D-G84-333-2
VENUS
EARTH
JUPITER
SATURN
ELECTRIC FIELD
SPECTRAL DENSITY (V²/m² Hz)
f_ce
f_pi
f_B
V_sw / 2πλ_D
f_pe
PIONEER
IMP-6
VOYAGER
VOYAGER
FREQUENCY (Hz)

Figure 4

C-G84-1023

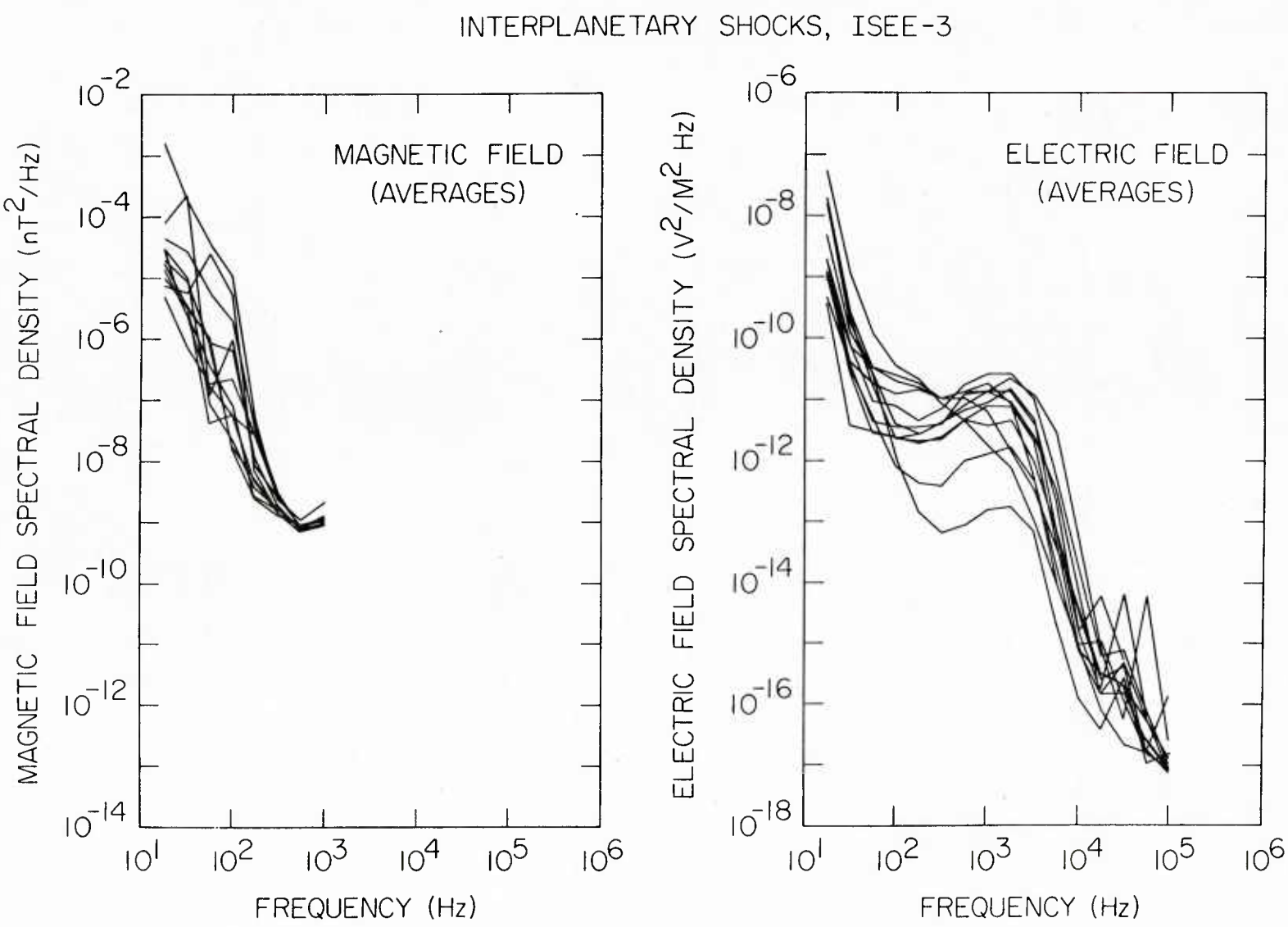

Figure 5

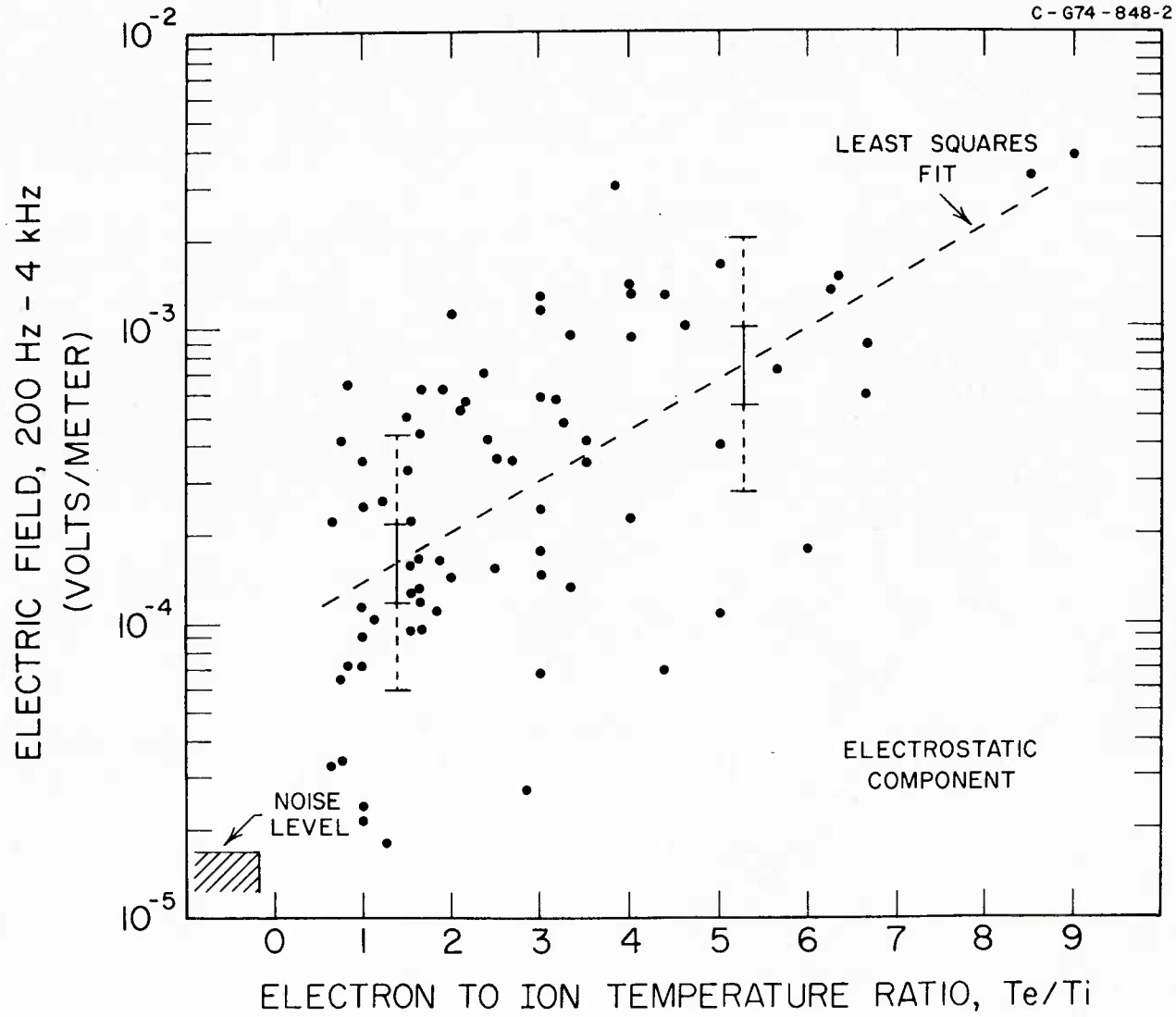
C-G74-848-2
ELECTRIC FIELD, 200 Hz - 4 kHz
(VOLTS/METER)
10^{-2}
10^{-3}
10^{-4}
10^{-5}
LEAST SQUARES
FIT
ELECTROSTATIC
COMPONENT
NOISE
LEVEL
0 1 2 3 4 5 6 7 8 9
ELECTRON TO ION TEMPERATURE RATIO, Te/Ti

Figure 6

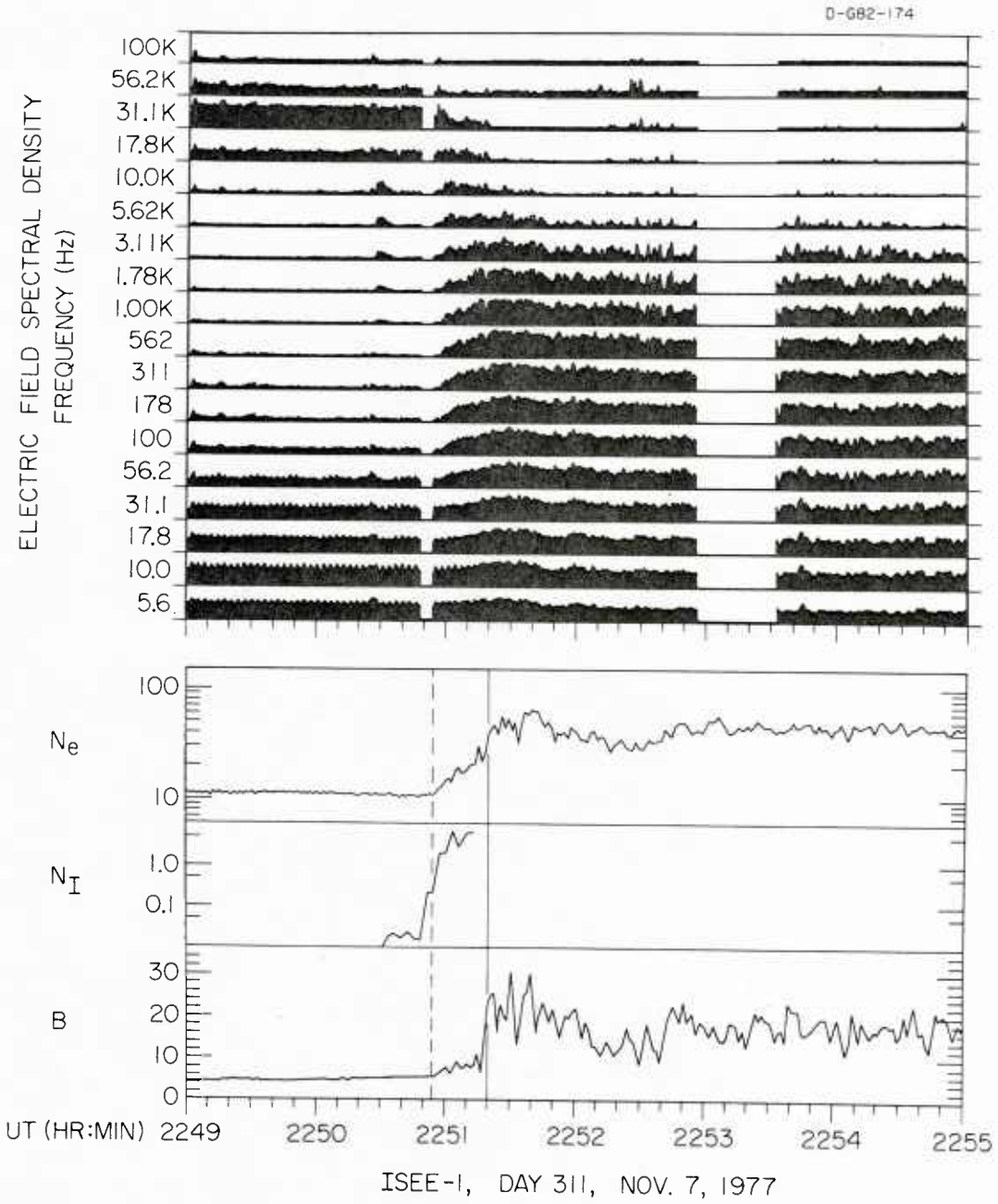
D-G82-174
ELECTRIC FIELD SPECTRAL DENSITY
FREQUENCY (Hz)
100K
56.2K
31.1K
17.8K
10.0K
5.62K
3.11K
1.78K
1.00K
562
311
178
100
56.2
31.1
17.8
10.0
5.6
N_e
100
10
N_I
1.0
0.1
B
30
20
10
0
UT (HR:MIN) 2249
2250
2251
2252
2253
2254
2255
ISEE-1, DAY 311, NOV. 7, 1977

Figure 7

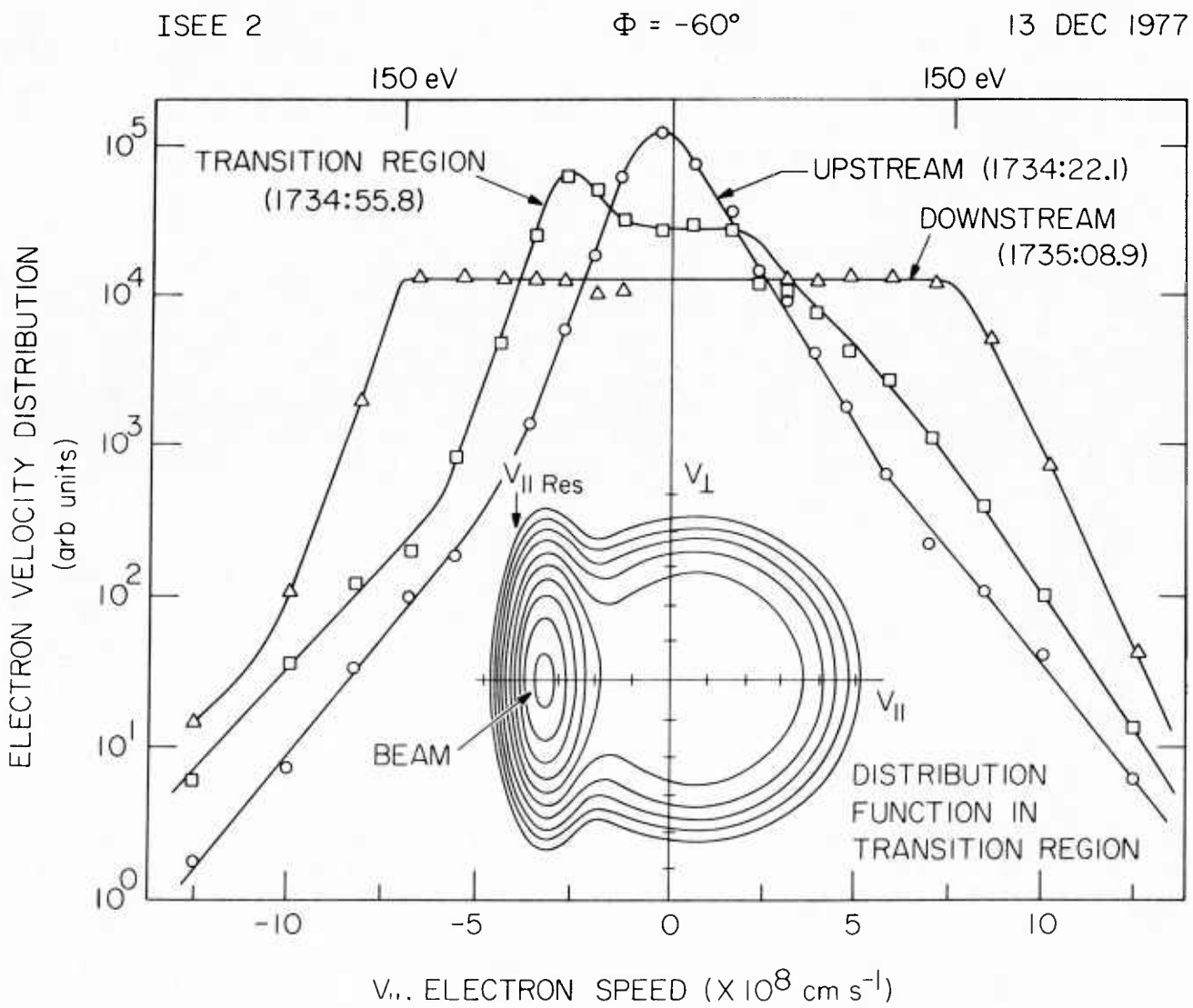
ISEE 2
Φ = -60°
13 DEC 1977
150 eV
150 eV
TRANSITION REGION
(1734:55.8)
UPSTREAM (1734:22.1)
DOWNSTREAM
(1735:08.9)
ELECTRON VELOCITY DISTRIBUTION
(arb units)
10^5
10^4
10^3
10^2
10^1
10^0
V_{II} Res
$V_\perp$
V_{II}
BEAM
DISTRIBUTION
FUNCTION IN
TRANSITION REGION
-10
-5
0
5
10
V_{II}, ELECTRON SPEED ($\times 10^8$ cm s^{-1})

Figure 8

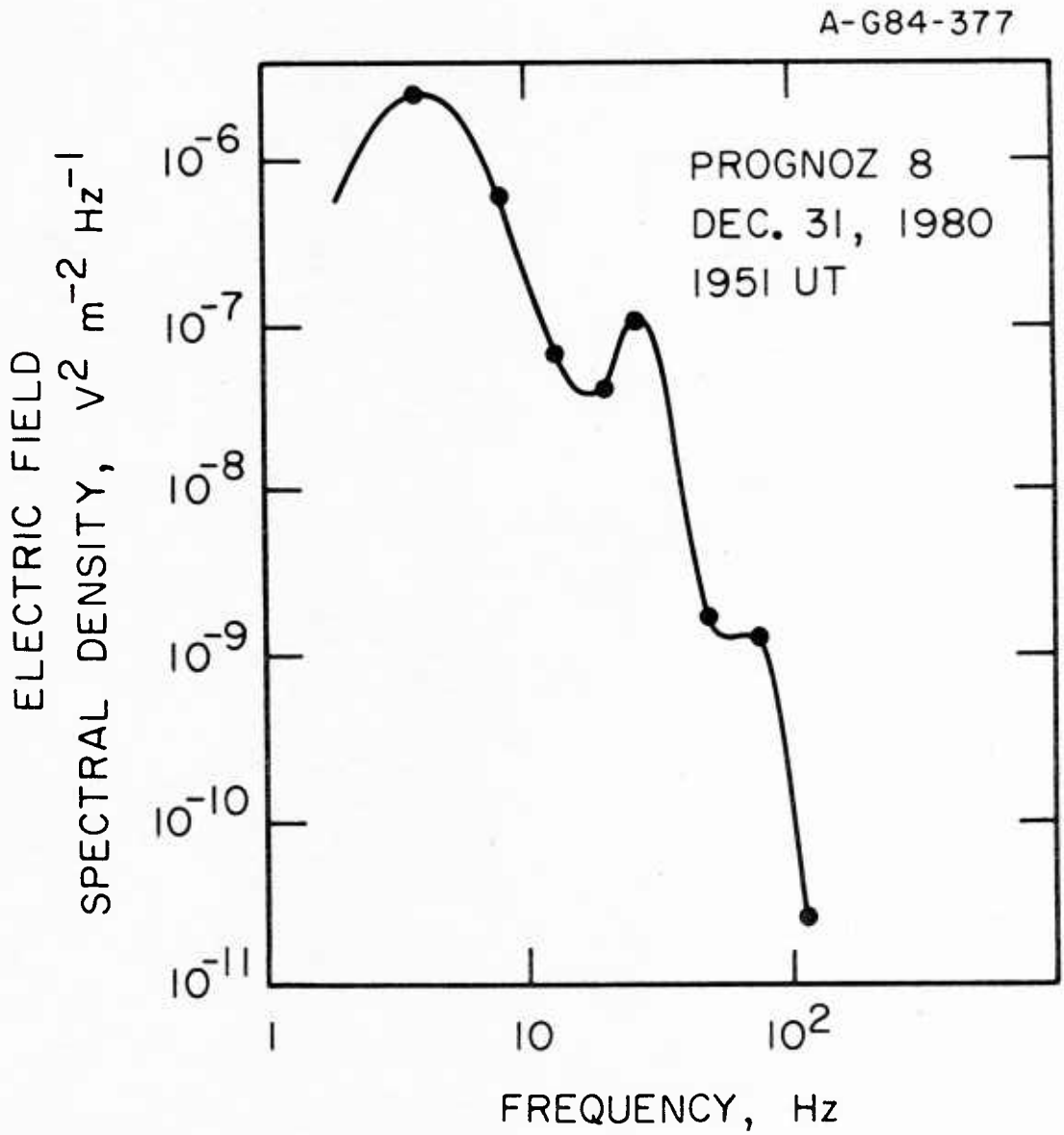
A-G84-377
PROGNOZ 8
DEC. 31, 1980
1951 UT
ELECTRIC FIELD
SPECTRAL DENSITY, V² m⁻² Hz⁻¹
10⁻⁶
10⁻⁷
10⁻⁸
10⁻⁹
10⁻¹⁰
10⁻¹¹
1
10
10²
FREQUENCY, Hz

Figure 9

A-G84-579

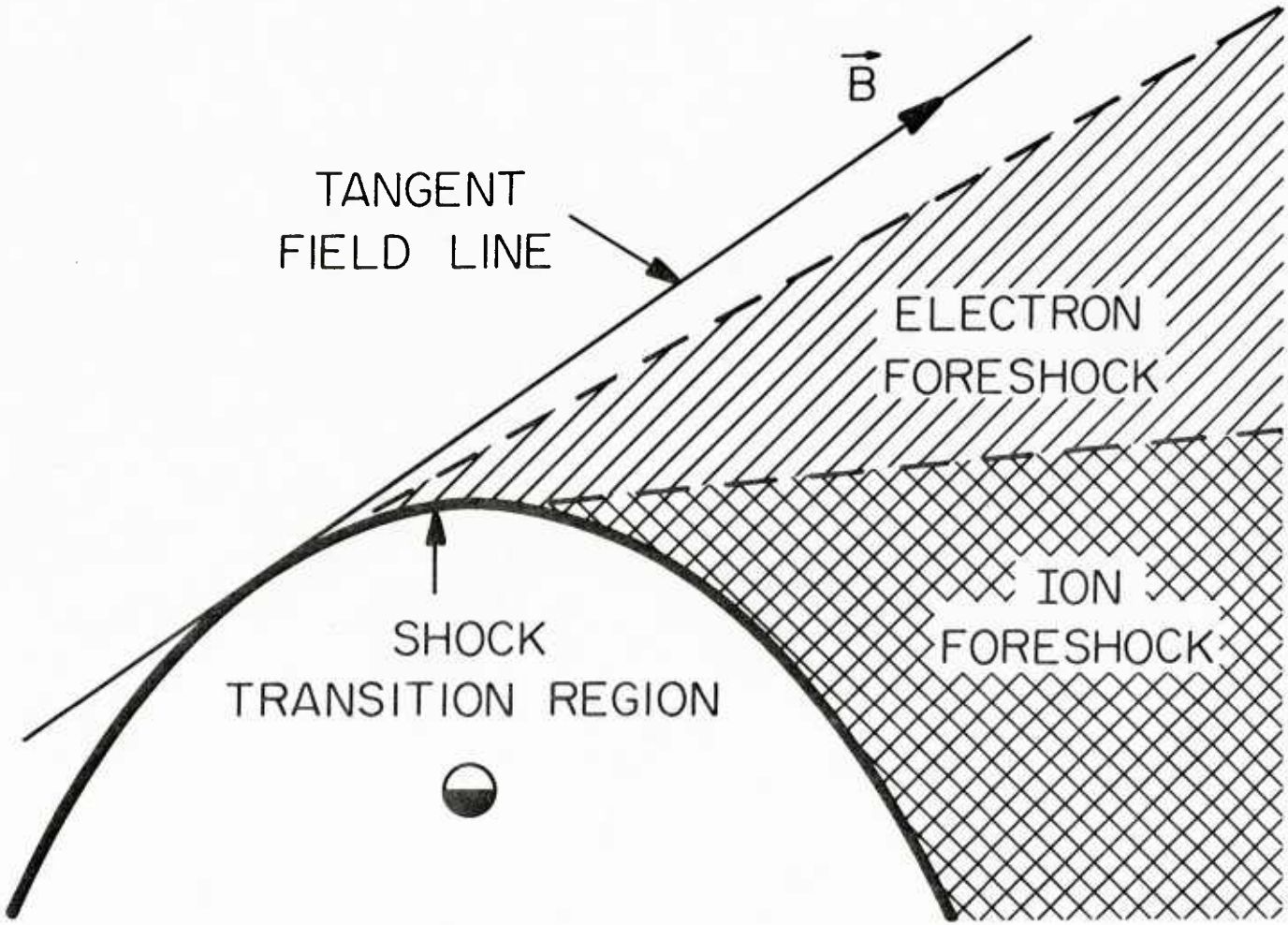

Figure 10

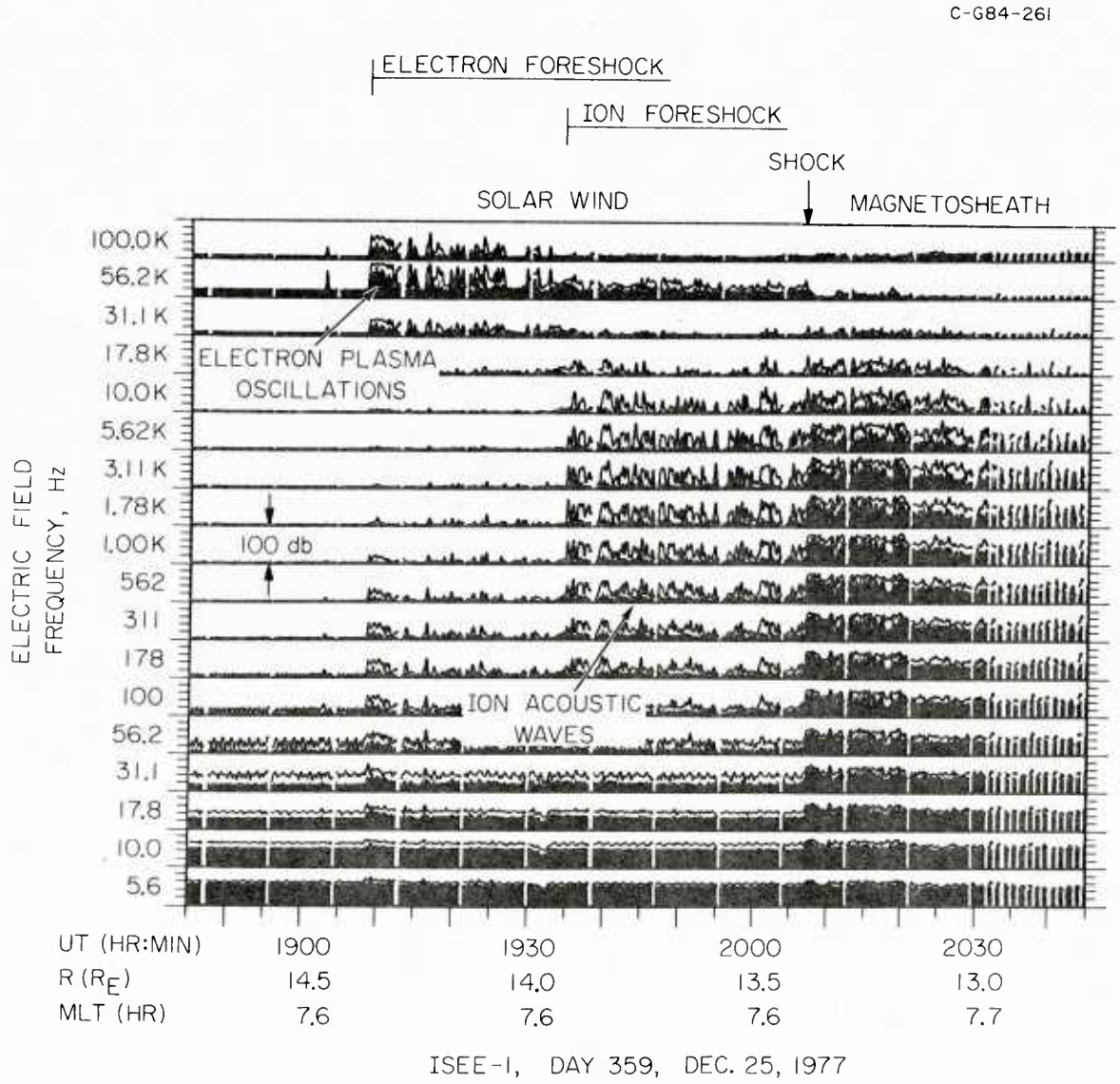
C-G84-261
ELECTRON FORESHOCK
ION FORESHOCK
SHOCK
SOLAR WIND
MAGNETOSHEATH
100.0K
56.2K
31.1K
17.8K
10.0K
5.62K
3.11K
1.78K
1.00K
562
311
178
100
56.2
31.1
17.8
10.0
5.6
ELECTRIC FIELD
FREQUENCY, Hz
ELECTRON PLASMA
OSCILLATIONS
100 db
ION ACOUSTIC
WAVES
UT (HR:MIN) 1900 1930 2000 2030
R (R_E) 14.5 14.0 13.5 13.0
MLT (HR) 7.6 7.6 7.6 7.7
ISEE-1, DAY 359, DEC. 25, 1977

Figure 11

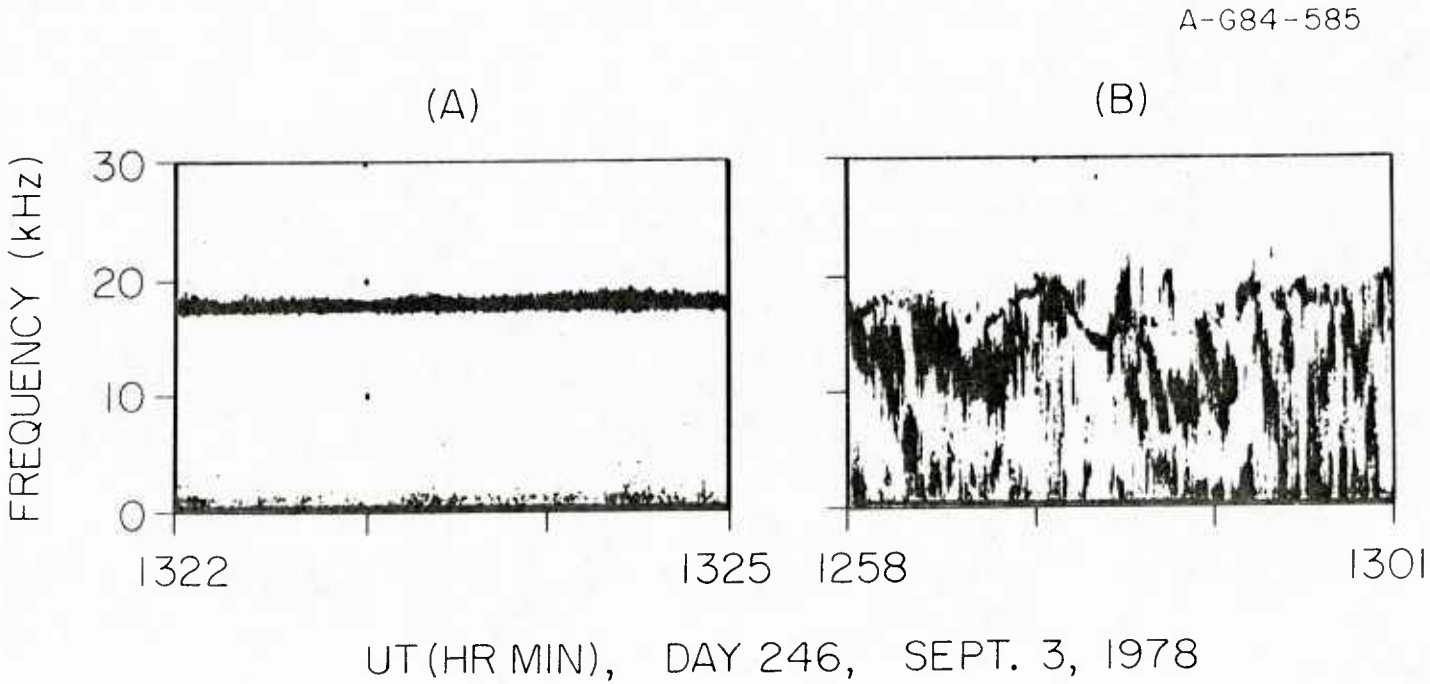
A-G84-585
(A)
(B)
FREQUENCY (kHz)
30
20
10
0
1322
1325
1258
1301
UT (HR MIN), DAY 246, SEPT. 3, 1978

Figure 12

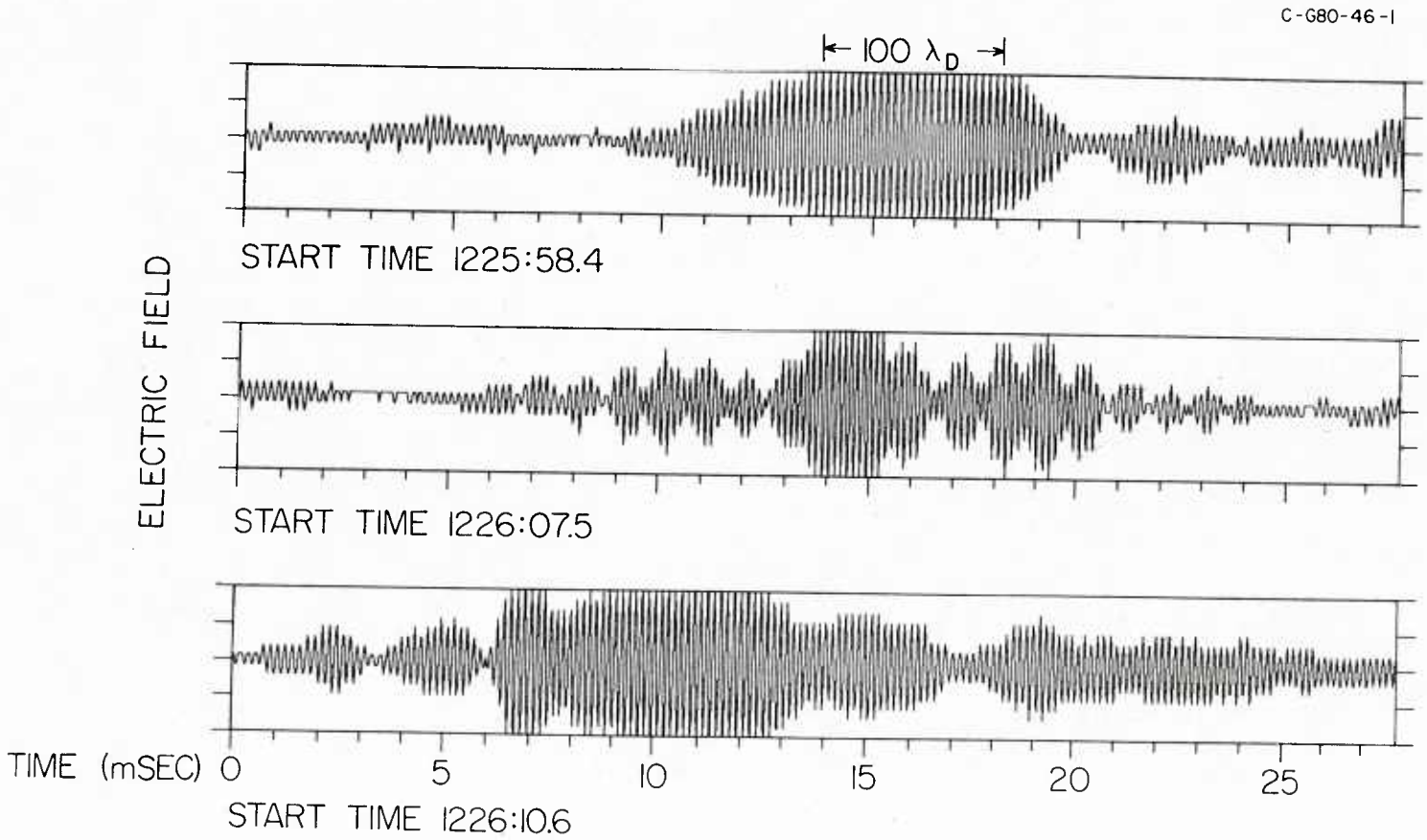
C-G80-46-1
← 100 λD →
START TIME 1225:58.4
START TIME 1226:07.5
START TIME 1226:10.6
ELECTRIC FIELD
TIME (mSEC) 0
5
10
15
20
25

Figure 13

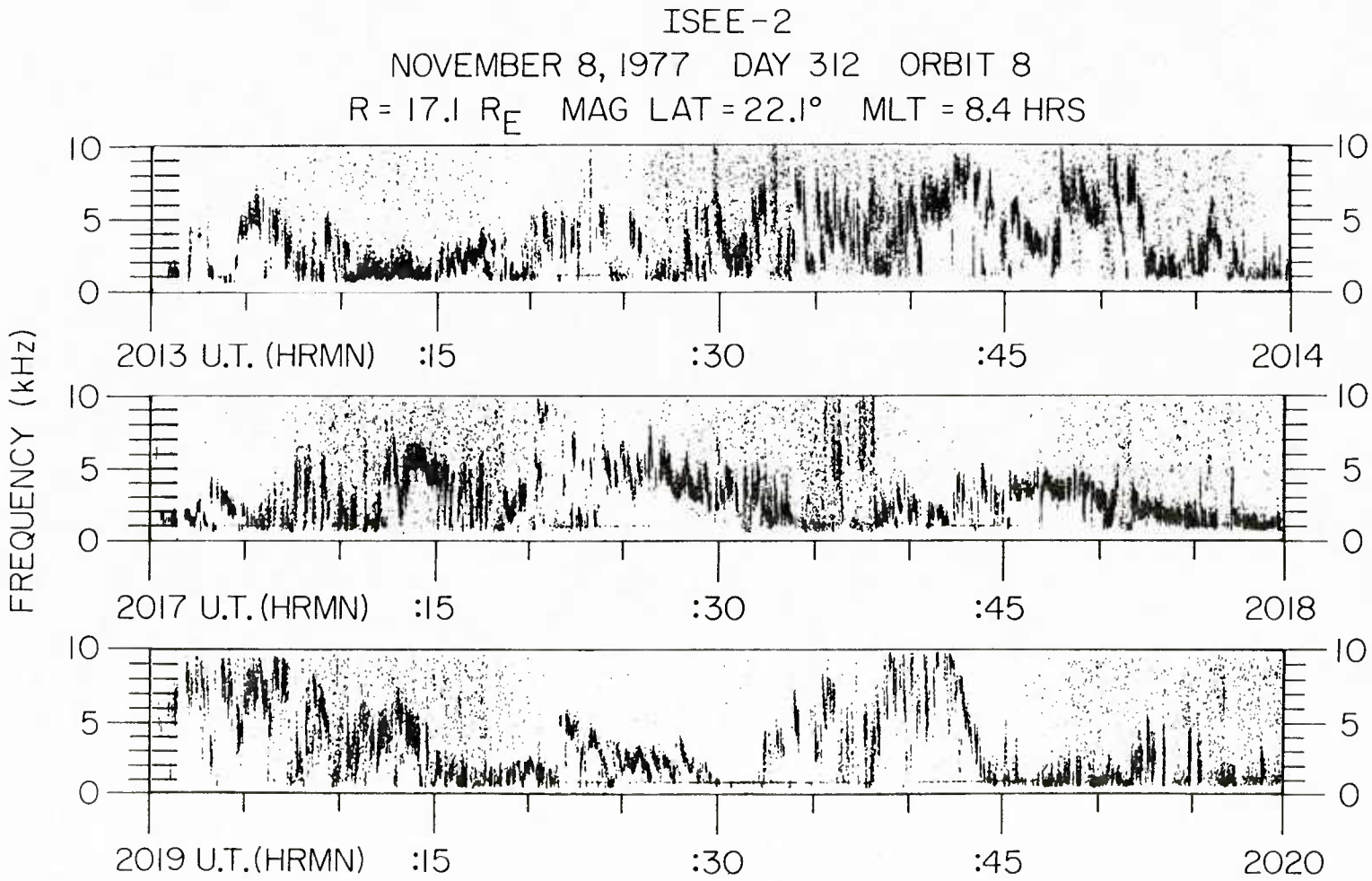
ISEE-2
NOVEMBER 8, 1977 DAY 312 ORBIT 8
R = 17.1 R_E MAG LAT = 22.1° MLT = 8.4 HRS
FREQUENCY (kHz)
10
5
0
2013 U.T. (HRMN)
:15
:30
:45
2014
2017 U.T. (HRMN)
2018
2019 U.T. (HRMN)
2020

Figure 14

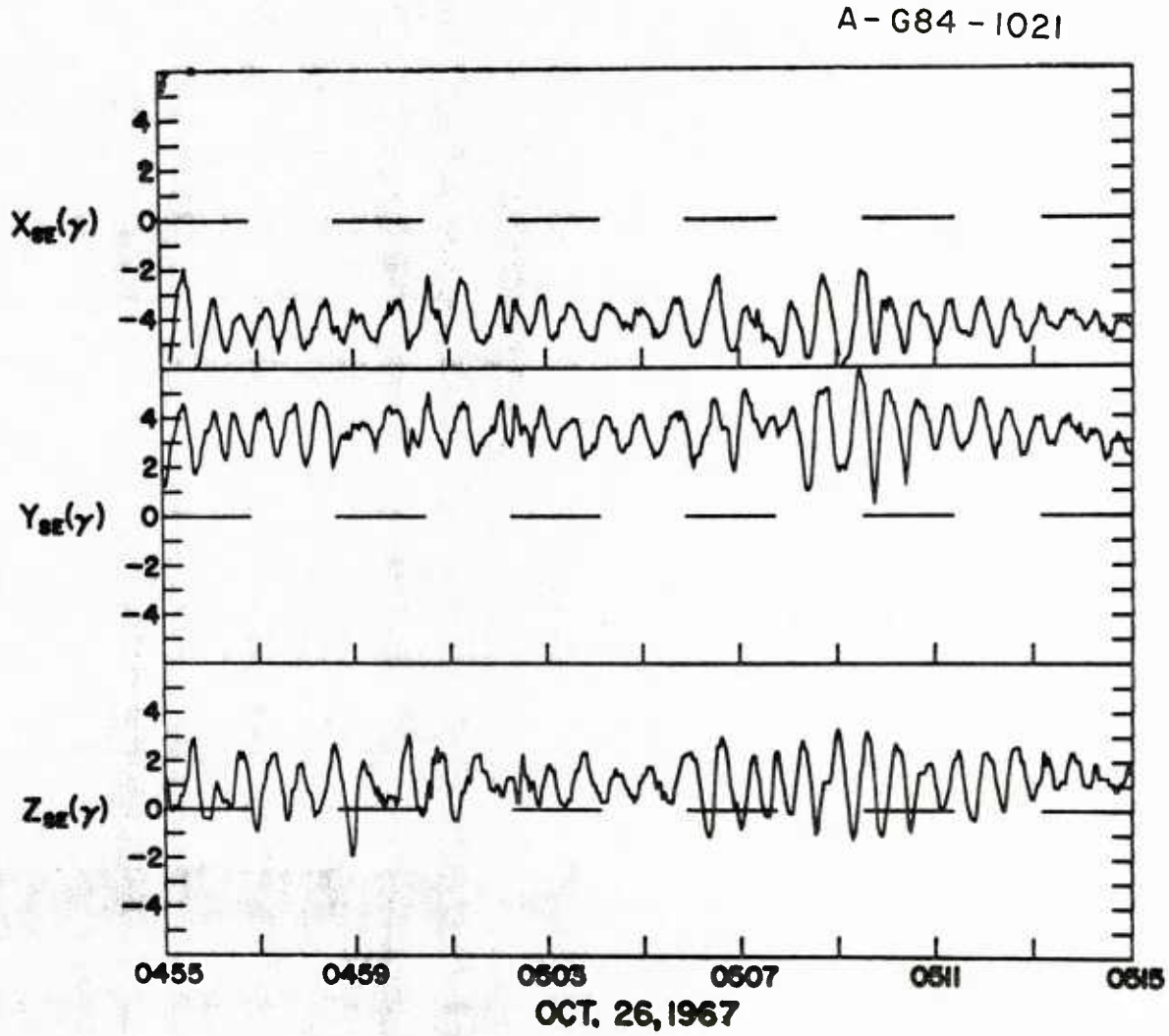
A-G84-1021
$X_{SE}(\gamma)$
$Y_{SE}(\gamma)$
$Z_{SE}(\gamma)$
4
2
0
-2
-4
0455
0459
0503
0507
0511
0515
OCT. 26, 1967

Figure 15